Title

Dissection of MAPK signaling specificity through protein engineering in a developmental context

Diego L. Wengier[1*], Gregory R. Lampard[1] and Dominique C. Bergmann[1,2,*]

[1] Howard Hughes Medical Institute and [2]Stanford University, Department of Biology, 371 Serra Mall, Stanford, CA 94305, USA.

* Corresponding authors: dbergmann@stanford.edu and dwengier@dna.uba.ar

Running title: Rewiring of MAPK cascades in Arabidopsis

Key words: MAPK specificity/Signal Transduction/Network rewiring/Stomatal development

Subject Categories: Synthetic Biology and Plant Biology

Total Character count: 57,660

Figures: 9

Tables: 1

Figure supplements: 7

Supplemental Files: 1

Footnotes

1

The authors responsible for distribution of materials integral to the findings presented in this article are

Dominique C. Bergmann dbergmann@stanford.edu and dwengier@dna.uba.ar

Rewiring of MAPK cascades in Arabidopsis

1   **Abstract**

2

3   Mitogen-activated protein kinases (MAPK) signaling affects many processes, some of which

4   have different outcomes in the same cell. In Arabidopsis, activation of a MAPK cascade consisting of

5   YODA, MKK4/5 and MPK3/6 inhibits early stages of stomatal developmental, but this ability is lost at

6   the latest stage when guard mother cells (GMCs) transition to guard cells (GCs). Rather than

7   downregulating cascade components, stomatal precursors must have a mechanism to prevent late stage

8   inhibition because the same MKKs and MPKs mediate other physiological responses. Here, we

9   artificially activated the MAPK cascade using MKK7, another MKK that can modulate stomatal

10   development, and found that inhibition of stomatal development is still possible in GMCs. This suggests

11   that MKK4/5, but not MKK7, are specifically prevented from inhibiting stomatal development. To

12   identify regions of MKKs responsible for cell-type specific regulation, we used a domain swap approach

13   with MKK7 and a battery of *in vitro* and *in vivo* kinase assays. We found that N-terminal regions of

14   MKK5 and MKK7 establish specific signal-to-output connections like they do in other organisms, but

15   they do so in combination with previously undescribed modules in the C-terminus. One of these modules

16   encodes the GMC-specific regulation of MKK5, that when swapped with MKK7's, allows MKK5 to

17   mediate robust inhibition of late stomatal development. Because MKK structure is conserved across

18   species, the identification of new MKK specificity modules and signaling rules furthers our understanding

19   of how eukaryotes create specificity in complex biological systems.

20

21

22   **Introduction**

23   MAPKs have strategic roles in signal processing, in mediating stress responses, and in guiding

24   cell fate transitions and development (Keshet and Seger, 2010; Rodriguez et al., 2010; Yang et al., 2013;

25   Chen and Thorner, 2007). MAPK networks consist of a three-tiered cascade whose kinases--MAPK

26   kinase kinase or MKKK, MAPK kinase (Mapk/Erk kinases or MEK in animals, MKK in Arabidopsis)

27 and MAPK (MPK in Arabidopsis) sequentially phosphorylate and activate each other upon signal

28 perception. Downstream effectors may respond to MPK-mediated phosphorylation by changes in protein

29 activity, localization or stability, and many of these alterations ultimately alter transcriptional programs.

30 The MKK level is a bottleneck in many species. In humans, at least 25 MKKKs activate the 7 MEKs,

31 which lie upstream of 14 MAPKs (Keshet and Seger, 2010). In *Arabidopsis thaliana*, more than 60

32 MKKKs are predicted upstream of 10 MKKs and 23 MPKs (Dóczi et al., 2012). Evidence exists that

33 MKKs can activate more than one MPK, and a given MPK may have more than one upstream MKK

34 (Andreasson and Ellis, 2010). Intuitively, this arrangement could facilitate signal integration, as multiple

35 signals could converge on a single effector. The use of common components, however, could also lead to

36 erroneous cross-activation.

37   When expressing multiple MAPK network components and responding to multiple sources of

38 information, how do cells generate an appropriate output to a particular signal? One strategy is to make

39 downstream effectors available in only certain cells (Lampard et al., 2008) or under certain conditions

40 (Bao et al., 2004; Brückner et al., 2004; Chou et al., 2004). Alternatively, signaling networks can be

41 insulated through the use of scaffolds, subcellular partitioning of signaling complexes, and by varying

42 signal amplitude or duration (Murphy et al., 2003; Murphy and Blenis, 2006; Raman et al., 2007; Keshet

43 and Seger, 2010; Good et al., 2011; Dóczi et al., 2012). Some MAPK network components encode

44 regions that allow them to establish these connections or localizations. For instance, the animal MEK1/2

45 uses its proline-rich sequence (PRS) to bind the scaffolds Kinase Suppressor of Ras (KSR) and Mek

46 Partner 1 (MP1). Binding to MP1, in particular, mediates endosomal localization (Schaeffer et al., 1998;

47 Teis et al., 2002; McKay et al., 2009). Several human MEKs and all Arabidopsis MKKs lack a PRS,

48 however, leaving questions about how these smaller MKKs are correctly assembled into restricted MAPK

49 networks.

50   In Arabidopsis, MAPK signaling has been shown to have a fundamental role in the formation of

51 stomata, the structures in the epidermis of plants that regulate gas exchange (Bergmann et al., 2004;

52 Wang et al., 2007). A systematic study of cell stage-specific responses to MAPK activation revealed that

4

53 stomatal precursors have mechanisms to limit certain cellular outputs and generate MKK-specific

54 responses (Lampard et al., 2009, 2014). Only four of the 10 MKKs -MKK4, MKK5, MKK7 and MKK9-

55 have any capacity to influence stomatal development during lineage initiation, guard mother cell (GMC)

56 commitment and/or guard cell (GC) formation (for simplicity, only MKK5 and MKK7 are shown in

57 Figure 1). Expression of any of these four constitutively active (CA) MKKs strongly inhibits stomatal

58 formation in early development (Figure 1A, C and D). At the last stage of development, however, MKK4

59 and MKK5 lose their ability to inhibit stomatal formation (Figure 1B and E). MKK7 and MKK9

60 activation, in contrast, results in stomatal clustering (Figure 1B and F). Loss of function studies with

61 *MKK4* and *MKK5* indicate that these kinases are endogenously required to limit stomatal production

62 (Wang et al., 2007), but the MKK7/9 significance is unclear as *mkk9* single mutants do not affect stomata

63 and in the recent report of true loss of function mutations in *mkk7* mutants no stomata phenotype was

64 described (Jia et al., 2016).

65

66 **Figure 1: Schematic of stomatal lineage, indicating stages where MKK activation leads to similar**

67 **and divergent outputs (based on** (Lampard et al., 2009)**).** (A-B) Diagrams of MAPK signaling cascades,

68 with each colored circle representing a different kinase level; circles are labeled with relevant kinase

69 number, with orange circle representing MPK of unknown identity. Constitutive activation of YDA

70 (MKKK), MKK5 or MKK7 inhibits stomatal lineage initiation (A, SPCH and MUTE stages). Late in the

71 lineage (B, FAMA stage) YDA and MKK7, but not MKK5, activation leads to stomatal proliferation via

72 an unidentified MPK. (C-F) Tracings of phenotypes resulting from activation of kinases. In C-D,

73 constitutively active MKK5 (MKK5^{DD}) or MKK7 (MKK7^{ED}) inhibit initiation (division of meristemoid

74 mother cell (MMC) into meristemoid (M)) and lineage progression (conversion of M into guard mother

75 cell (GMC)). In E-F, MKK5^{DD} has no effect (E, WT numbers and distribution of stomata in green), but

76 MKK7^{ED} induces guard cell (GC) overproliferation and clustering (F). Stages are referred to as SPCH,

77 MUTE and FAMA after the promoters to drive expression of MAPK network components (Lampard et

78 al., 2009). YDA, YODA; 5, MKK5; 7, MKK7; 3/6, MPK3 and MPK6.

79

80   MKK4/5's endogenous role in limiting stomatal production in early stages, but not in late

81 stomatal lineage cells, provides an excellent test case for examining how cell identity may interface with

82 signaling response. We created a quantitative phenotypic analysis pipeline that revealed a previously

83 underappreciated capacity for late stage stomatal lineage cells to be inhibited by MAPK signaling. Then,

84 taking advantage of divergent responses to constitutively activated MKK5 and MKK7, we implemented a

85 protein engineering approach to identify structural domains in MKK5 that are responsible for its stage-

86 specific behaviors. We found that MKK N-terminal regions establish specific signal-to-output

87 connections, much like they do in other organisms (Won et al., 2011), but this requires coordination with

88 previously unexplored regions in the C-terminus. We also found that a minimal domain in the C-terminus

89 encodes the basis for MKK-specific regulation. The location of specificity modules within the plant

90 proteins corresponds to regions in which their human homologues display high sequence diversity,

91 suggesting that these regions may contribute to specificity in many situations. Given the global

92 conservation of MAPK signaling, our findings in the complex multicellular context of plant development

93 may offer insights into general mechanisms of signaling specificity in complex biological systems.

94

95

96 **Materials and Methods**

97

98 **Plant material and growth conditions**

99   All transgenic lines were generated in the Col-0 background. Seeds were plated on 0.5X

100 Murashige-Skoog media containing 1% agar-agar (Caisson Laboratories, North Logan, UT) and 100

101 μg/ml Kanamycin (Sigma-Aldrich) or 50 μm/ml Hygromycin B (Life Technologies) when appropriate.

102 Seedlings were grown under a light intensity of 100 μmol photons m^{-2} s^{-1} in a 16:8 photoperiod at 22 ±

103 1ºC. Analyses were performed in 15 day after germination (dag) cotyledons unless stated otherwise. The

104   *mpk6-3* allele was Salk_127507 (Müller et al., 2010). Mutant alleles for *EDR1* (Salk_127158), *MAP3Kδ1*

105   (Salk_048985) and *MAP3Kδ5* (Salk_029929 and Salk_036615) were obtained from the ABRC.

106

107   **Multiple sequence alignment and structural analysis**

108   Selected mammalian kinases were aligned using ClustalOmega (Sievers et al., 2011) and

109   structural models are in Supplemental Figure 3B. MKK5 and MKK7 structural predictions were

110   performed with I-Tasser (Zhang, 2008), using MEK1 (1S9J) to assist the prediction. Models were

111   explored with Swiss-PdbViewer v4.1 and fit with the Magic Fit button (Guex and Peitsch, 1997).

112   Structural features were extracted from models and overlaid on the primary sequence (Supplemental

113   Figures 3-5).

114

115   **Construction of constitutively active MKK and synthetic chimeras**

116   Domain swap constructs were assembled by fusion PCR from DNA amplicons (blocks) generated

117   with Phusion® High-Fidelity DNA Polymerase following manufacturer's instructions (New England

118   Biolabs, Ipswich, MA). To generate blocks, MKK5^{DD} and MKK7^{ED} cloned into pENTR without stop

119   codons or other chimeras were used as templates (Lampard et al., 2009). Blocks were designed to contain

120   attL1 and attL2 functional sequences from pENTR to ease the cloning procedure through the Gateway

121   strategy (Supplemental File 1). For domain swaps assembled from two blocks, 5' blocks contained the

122   M13 forward priming site and attL1 recombination site before the MKK sequence; and 3' blocks

123   contained the MKK sequence followed by attL2 recombination site and M13 reverse priming site. To

124   facilitate fusion of the blocks, reverse primers for 5' blocks and forward primers for 3' blocks were

125   designed as chimeras of the two blocks to be fused, containing at least 15 bases from each block, and

126   were completely complementary to each other. PCR products were gel extracted using QIAquick Gel

127   Extraction Kit (QIAGEN Inc., Valencia, CA) and 1:1 molar ratio mix were used as templates on fusion

128   PCR reactions using M13 forward and reverse primers. Domain swap constructs were gel purified and

129   cloned into pJET 1.2 according to CloneJET PCR Cloning Kit instructions (Thermo Life Sciences,

130   Pittsburgh, PA). For domain swap constructs assembled from 3 blocks, 5' and 3' were generated with the

131   same strategy as above, while internal block was amplified with forward and reverse chimeric primers. As

132   domain swaps became more elaborate, first domain swap constructs were used as templates for generating

133   new blocks. Primers, templates and sequences for each domain swap are listed in Supplemental Table 1,

134   A and B.

135   To build constructs for expression under SPCH and FAMA promoters, 2.5-kb fragments

136   previously described (Ohashi-ito and Bergmann, 2006; Macalister et al., 2007) were first adapted to the

137   Multisite Gateway system. Promoters were shuttled from pENTR to pDONR P4 P1R (Life Technologies,

138   Grand Island, NY) by PCR amplification using promoter shuttling primers (Supplemental File 1)

139   followed by BP recombination performed under manufacturer's instructions. Promoters flanked by attL4

140   and attR1 recombination sites (pDONR-promoter) were used in Multisite recombination reactions with

141   domain swap constructs in pJET and R4pGWB440 [destination vector carrying the Gateway cassette

142   flanked by attR4 and attR2 recombination sites, in frame C-terminal fusion to enhanced YFP and

143   kanamycin selection in plants (Nakagawa et al., 2008)]. Recombination reactions were performed in a

144   two-step protocol. First, 1 µl of LR Clonase II was added to 4 µl vector mix (containing 150 ng of

145   pDONR-promoter and 150 ng pJET-domain swap construct) and incubated at 25ºC for 5 hours. Then, 150

146   ng of R4pGWB440 in 4 µl solution were added to the reactions along 1 µl of LR Clonase II. Reactions

147   were incubated for additional 16 hours at 25ºC and then stopped after the addition of 1 µl of Proteinase K

148   and incubation for 10 min at 37ºC. Constructs were confirmed by sequencing and introduced in

149   Arabidopsis by *Agrobacterium tumefaciens*-mediated transformation.

150   Mutants *edr1*, *map3kδ1* and *map3kδ5* were transformed with *FAMA$_{pro}$:MKK5^{DD}* in pHGY,

151   previously used in (Lampard et al., 2009). MPK3 and MPK6 clones were provided by Jean Colcombet

152   (INRA Versailles-Grignon, France) (Berriri et al., 2012).

153

154   **Scoring phenotypes and data analysis**

155   Seedlings (15 dag) were fixed in 7:1 ethanol:acetic acid, and cleared in Hoyer's medium.

156   Cotyledons were imaged by differential interference contrast microscopy on a Leica DM2500 microscope

157   at ×20 magnification (0.320 mm^{-2} field of view). One picture per independent transgenic seedling was

158   taken from the distal tip of the cotyledons, within the vascular loop, on the abaxial epidermis. Phenotypes

159   at the FAMA stage were as follows: (1) normal phenotype, only single stomata with tolerance for 1

160   stomatal cluster per field of view; (2) stomatal inhibition, no stomata present or inhibited precursors

161   coexisted with normal stomata and appeared in at least two independent fields of view per sample; (3)

162   large stomatal cluster, at least two stomatal clusters (4 or more stomata in contact) per field of view; (4)

163   small stomatal cluster, clusters contained 2-3 stomata in contact. When a sample contained a mixed

164   population of clusters, the presence of large clusters defined the classification for this category. MKK7^{ED},

165   clusters were systematically bigger than any chimera and often were delayed in development; to confirm

166   clustering, older epidermis (near apical hydathode or in older plants) was scored. SPCH stage phenotypes

167   were quantified as (1) inhibited (no stomata per field of view) or (2) not inhibited (2 or more stomata per

168   field of view). To enable us to score phenotypes in T1 seedlings that must be grown on antibiotic

169   selection, we grew 35S:YFP lines with the same antibiotic resistance as the MKK variants under the same

170   conditions and scored these as the equivalent of WT controls.

171   A binomial distribution for phenotypic data was assumed and the percentages of each phenotype

172   were calculated with a confidence of 95%. This analysis is similar to others done on data of comparable

173   nature (Wang et al., 2011). Linear regressions between *in vitro* and *in vivo* data; and between SPCH and

174   FAMA data in Figure 7 and Supplemental Figure 7 were done with Microsoft Excel. To cluster chimeras,

175   hierarchical clustering was performed on phenotypic data at the FAMA stage using the function pvclust in

176   the statistical software R. Percentages of each one of the four phenotypes -Inhibited, Normal, Small

177   Clusters and Large Clusters- were converted to frequencies (e.g. dividing by 100). The distance matrix

178   was obtained by calculating the dissimilarities between all chimeras in their four phenotypes with the

179   Manhattan method. Clustering was performed with the ward.d method and the number of bootstrap

180   replications was 1000. To statistically determine how similar chimeras were within clusters, a Chi-

181 squared test of independence was implemented to compare phenotype distributions. Frequencies were

182 compared to YFP (inactive), MKK5^{DD}, MKK7^{ED} (inhibition of stomatal formation and stomatal clustering)

183 and N5-MKK7^{ED} (strong stomatal inhibition). Chimeras that were not statistically different are noted with

184 the same number in Figure 7B. Unnumbered chimeras were statistically different from the rest (p < 0.05).

185

186 **Confocal microscopy**

187 Confocal images were collected using a Leica SP5 confocal microscope with excitation/emission

188 spectra of 514/520 to 540 for YFP and 565/580 to 610 for propidium iodide counterstaining. ImageJ (NIH)

189 was used to build Z-stacks from confocal images. To improve resolution of cell outlines, layers were

190 summed rather than averaged. Z-stacks were then split into single channels and only the channel for the

191 cell outlines was conserved, transformed into a grey-scale image and colors were inverted. Bright and

192 contrast were modified to improve image quality. For localization, color channels in Z-stacks were

193 maintained and images were cropped. Localization of MKK-YFP chimeras was investigated in stable

194 (T2-T3) lines with the exception of chimeras that induced stomatal inhibition, where localization was

195 determined in T1s on antibiotic selection.

196

197 **Kinase-inactive MPK3 and MPK6 phosphorylation**

198 *In vitro* kinase assays to assess the ability of MKK variants to phosphorylate either kinase

199 inactive (KI) MPK3 or MPK6 were performed as described in (Lampard et al., 2014). KI-MPKs were

200 used to avoid autophosphorylation of the substrates. Band intensity was detected and analyzed using

201 ImageJ (NIH). Each reaction was performed in triplicate. The ratio of phosphorylated KI-

202 MPK/unphosphorylated KI-MPK detected by p42/44 antibody (Cell Signaling, Cat. No. 9102) was used

203 to estimate MKK activity. Background signal corresponds to 1. Mean and standard error was calculated

204 for each sample.

205

206 **Yeast two-hybrid assays**

207   Yeast two-hybrid assays was performed with the matchmaker Two-Hybrid System 3 (Clontech)

208   using a modified set of plasmids compatible with Gateway technology and conditions specified by the

209   manufacturer. MKKs and chimeras were cloned as DNA Binding Domain fusions and MPKs were cloned

210   as Activation Domain fusions. Three independent yeast colonies were tested for each pairwise

211   comparison at 1, 1:10 and 1:100 dilutions after incubation of 2, 3 and 4 days in plates containing 1 mM 3-

212   amino-1/2/4-triazole. Experiments were repeated three times with yeast cultures at OD600 of 1, 2 and 4.

213   Interactions were evaluated as positive if significant growth was detected in 1:100 dilution at day 3.

214

215   **Accession Numbers**

216   Arabidopsis Genome Initiative locus identifiers for the genes studied in this work are: SPCH,

217   AT5G53210; FAMA, AT3G24140; MKK5, AT3G21220; MKK6, AT5G56580; MKK7, AT1G18350;

218   MPK3, AT3G45640; MPK6, AT2G43790; EDR1, AT1G08720; MAP3Kδ1, AT1G11850; MAP3Kδ5,

219   AT4G24480.

220

221

222   **Results**

223

224   **Stomatal development is inhibited by MAPK activation at the FAMA stage**

225   To carefully define the range of phenotypes in our system, we re-analyzed the inhibitory effect of

226   CA-MKK expression in FAMA stage cells (Figure 1B) using more sensitive and quantitative

227   measurements than in our previous studies (Lampard et al., 2009, 2014). For simplicity, we selected one

228   representative MKK from each MKK4/5 and MKK7/9 pair as previous studies showed that MKK4

229   mirrors MKK5 activity, and MKK7 mirrors MKK9 activity, in every stage of stomatal development

230   (Lampard et al., 2009, 2014). Because MKKs were to be analyzed *in planta*, we selected MKK5 and

231   MKK7, both of which can be easily detected as YFP fusion proteins, thereby providing a control for

232   expression. FAMA promoter (FAMApro) was used to drive the expression of constitutively active MKKs

11

233   which are made dominantly active by replacing the regulatory S/T residues of the activation loop with

234   phosphomimetic D/E residues (MKK5^{DD} = MKK5^{T215D,S221D} and MKK7^{ED} = MKK7^{S193E,S199D}) (Lampard

235   et al., 2009; Popescu et al., 2009). To be able to observe all epidermal phenotypes produced by different

236   MKK expression levels, such as inhibition of stomatal development and stomatal clustering, phenotypes

237   were quantified in cotyledons of independent primary transformants (T1s in Table 1, Figure 2A). We paid

238   special attention to evidence of seedling lethality, a typical result of inhibition of stomatal development.

239

240   **Figure 2: Differences phenotypic output between MKK5 and MKK7.** (A) Micrographs of phenotypes

241   resulting from FAMA-stage expression of MKK5^{DD} and MKK7^{ED}: inhibited GMCs, where precursors

242   exit the stomatal lineage and do not make GCs (arrowheads); Normal (single stomata comprised of two

243   GCs) or small (2-3) or large (4+) clusters of adjacent stomata resulting from overproliferation of

244   precursors before they become GCs. Scale bars are 10 μm. (B) Quantification of phenotypes, percentage

245   of seedlings showing one of four phenotypes. >19 independent transformants were scored per genotype

246   and stage (Ns reported in Table 1). 35Spro:YFP was used as a negative control (see Methods). Error bars

247   correspond to 95% confidence intervals.

248

249

250 **Table 1: Quantification of *in vivo* and *in vitro* phenotypes conferred by chimeras.**

Name	Kinase Activity (normalized to MKK5^{DD})				SPCH stage inhibition of linage initiation		FAMA stage phenotypes (as percentage of total T1 seedlings)					
	KI-MPK3		KI-MPK6		n	%	n	Inhibited	WT	GC clusters		
	AVG	SE	AVG	SE						Small	Large	Total
YFP control							24	0.00	91.67	8.33	0.00	8.33
MKK5^{DD}	34.485	9.052	38.259*	2.308	69	78.26	25	0.00	76.00	24.00	0.00	24.00
MKK7^{ED}	6.836	4.808	10.867	5.726	93	100.00	50	20.00	26.00	0.00	54.00	54.00
N7-MKK5^{DD}	5.500	1.894	21.448	9.176	75	26.67	125	8.80	32.00	48.80	10.40	59.20
N5-MKK7^{ED}	15.889	7.052	35.235*	1.457	22	86.36	47	93.62	6.38	0.00	0.00	0.00
MKK5^{DD}-C7	13.888	9.753	25.666*	2.530	47	87.23	44	65.91	29.55	4.55	0.00	4.55
MKK5^{DD}-7A	45.980	22.674	26.287	4.947	114	12.28	98	0.00	97.96	2.04	0.00	2.04
MKK5^{DD}-7B	46.746	22.671	38.718*	0.750	20	10.00	70	50.00	50.00	0.00	0.00	0.00
MKK7^{ED}-C5	3.877	2.091	0.728	0.148	43	13.95	19	0.00	78.95	21.05	0.00	21.05
MKK7^{ED}-CDR5	2.451	1.242	1.303*	0.312	89	98.81	30	96.67	3.33	0.00	0.00	0.00
MKK7^{ED}-CPR5	15.844	11.444	5.904	2.422	105	0.00	36	2.78	91.67	5.56	0.00	5.56
MKK7^{ED}-5A	15.440	12.606	5.219	4.017	125	88.00	54	81.48	14.81	3.70	0.00	3.70
MKK7^{ED}-5B	7.238	4.545	1.317	0.200	198	16.67	60	0.00	48.33	40.00	11.67	51.67
N7-MKK5^{DD}-C7	3.526	1.153	2.411	0.915	91	54.95	43	2.33	13.95	13.95	69.77	83.72
N5-MKK7^{ED}-C5	4.724	2.876	1.439	0.673	51	72.55	46	0.00	71.74	28.26	0.00	28.26
MPK3, not shown					49	0.00	50	0.00	82.00	18.00	0.00	18.00
MPK3$^{D193G/E197A}$					18	0.00	52	0.00	80.77	19.23	0.00	19.23
MPK3^{T119C}, not shown					43	0.00	89	0.00	86.52	13.48	0.00	13.48
MPK6, not shown					122	0.00	45	0.00	84.44	15.56	0.00	15.56
MPK6$^{D218G/E222A}$					6	100.00	27	0.00	77.78	22.22	0.00	22.22
MPK6^{Y144C}, not shown					35	0.00	21	0.00	90.48	9.52	0.00	9.52

251

252 Notes: Kinase activity is determined in triplicates with the exception of those marked with "*" that were done in duplicates. Averages (AVG) and

253 Standard Errors (SE) are represented in the table. Phenotypic categories for FAMA stage phenotypes are described in Methods.

254   Previously, expression of MKK7^{ED} was shown to lead to stomatal hyperproliferation (Lampard et

255   al., 2009), and we could confirm that result: 54% T1s showed large stomatal clusters (Figure 2A and B,

256   Table 1); however, 26% were WT (most of which showed no YFP signal) and 20% had stomatal

257   precursors that failed to complete their development into GCs (Figure 2A and B, Inhibited). This third

258   class died as seedlings. Among MKK5^{DD}-YFP transformants, there were no seedling lethals: 76% T1s

259   had a phenotype indistinguishable from controls (Figure 2B, Table 1) and 24% exhibited one to three

260   small clusters (2-3 stomata in contact) per 0.32 mm$^{2.}$. Among control seedlings grown in parallel, ~8%

261   exhibited similar small clusters (Table 1). Phenotype distributions for MKK5^{DD}-YFP and MKK7^{ED}-YFP

262   were statistically different in Chi-squared test of independence ($p \ll 0.05$).

263   These results indicate that MAPK activation through MKK7^{ED}, besides driving stomatal

264   clustering, can also lead to inhibition of stomatal development at the FAMA stage. The failure of

265   MKK5^{DD} to inhibit this stage transition is puzzling, since MKK5 is the endogenous kinase, whereas

266   MKK7 is not normally expressed in FAMA stage cells (Adrian et al., 2015). ,Moreover, MKK5^{DD} is an

267   effective inhibitor of earlier stages (Lampard et al., 2009) and *MKK4MKK5*RNAi lines show excess

268   mature GCs (Wang et al., 2007). Also, when compared to MKK7^{ED}, MKK5 exhibits stronger interactions

269   with MPK3/6 in Y2H (Supplemental Figure 1) and stronger kinase activity *in vitro* (Supplemental Figure

270   2). MKK5, therefore appears to be subject to an additional level of *in vivo* regulation that blocks its

271   inhibitory effect, while MKK7 seems to escape this regulation. We reasoned that structural differences

272   between MKK5 and MKK7 could be probed to define the nature and the source of this differential

273   regulation.

274

275   **Predicted tertiary structures of MKK5 and MKK7 suggest sources of MKK identity and specificity**

276   We reasoned that the domains most likely to confer the FAMA-stage differential responses would

277   be surface exposed (thus available for interactions with partners) and would exhibit the greatest structural

278   and sequence divergence among MKKs. To facilitate the identification of such regions, we modeled plant

279   MKK folds based on the X-ray crystal structures of human orthologs MEK1 and MEK2 using I-Tasser

280   (Zhang, 2008) (Figure 3) and used structural information from several other mammalian kinases (Hanks

281   and Hunter, 1995; Kannan and Neuwald, 2004; Goldsmith et al., 2007; Knight et al., 2007) to identify

282   conserved features.

283   Structural alignment of MKK5 and MKK7 to mammalian kinases confirmed the conservation of

284   the kinase fold (Knight et al., 2007) (Figure 3B and D, with primary sequence in Supplemental Figure

285   3A). The core catalytic domains of MKK5 and MKK7 are quite similar, but the N- and C-termini are

286   variable. This is similar to MEK1/2, where catalytic domains are similar and well resolved, but the

287   flanking N- and C- terminal extensions and a region containing the PRS are not. In addition, MKK5

288   possesses, but MKK7 completely lacks, sequences at positions comparable to the C-terminal extension in

289   MEK1/2 (Supplemental Figure 3C). Previously, we showed that this C-terminal extension does not

290   contribute to MKK5 activity or specificity, but that N-termini have an important role in MKKs activities,

291   possibly through the presence of D-docking domains that mediate interactions with downstream MPKs

292   (Lampard et al., 2014).

293

294   **Figure 3: Differences in protein structure between MKK5 and MKK7.** (A-D) Schematic and

295   predicted structures of MKK5 (blue) and MKK7 (red). CPR, C-terminal proximal region. CDR, C-

296   terminal Distal Region. (C-D) Four regions important for this study (N-termini, Loop A, Loop B and the

297   C-termini) are bolded. Conserved α helices A, F and G are labeled in grey.

298

299   In addition to the distinct C-terminal distant region (CDR), divergent surface-exposed regions of

300   the plant MKKs include a C-terminal proximal region (CPR) between conserved subdomains VIII and X

301   (Figure 3, Supplemental Figure 3 and 4). The CPR contains two loops. Loop A starts immediately

302   downstream of the YM(S/A)PER sequence, a MKK signature (Rodriguez et al., 2010), and ends before

303   the highly conserved α-helix F. The sequence of loop A is similar between kinases with identical

304   functions and different between kinases with divergent functions in both Arabidopsis and humans

305   (Supplemental Figure 4). For example, loop A in MKK4 and MKK5 is identical, whereas it differs

306   between MKK5 and MKK7. Loop B is downstream of α-helix F and displays a high tolerance for

307   sequence variability (Figure 3, Supplemental Figure 3 and 4). Among CMGC (<u>C</u>yclin-dependent kinases,

308   <u>M</u>APK, <u>G</u>lycogen synthase kinase and <u>C</u>yclin-dependent kinase-like kinase) group kinases, loop B

309   contains an insert that binds interacting proteins (Kannan and Neuwald, 2004), and a different insert in

310   MEK1/2 mediates binding to MAPK scaffolds MP1 and KSR (Schaeffer et al., 1998; Brennan et al.,

311   2011). This region is shorter in plant MKKs (making them resemble human MEK3-MEK7), but the

312   sequence divergence among MKKs is consistent with this loop being a specificity or identity determinant.

313   It is therefore a prime region to target in our dissection of specificity.

314

315   **N-termini link specific MKKs to specific phenotypes**

316   Different *in vivo* behaviors of MKK5^{DD} and MKK7^{ED} make it possible to begin to correlate

317   unique sequences and structures with unique functions. Informed by the structural analysis, we made

318   chimeric MKKs based on dividing the MKKs into N- terminal (N), kinase domain (MKK) and C-terminal

319   (C) regions, and further dividing the C domain into CDR and CPR (and within CPR, domain A and B)

320   (Figure 3). To assay the function of these domains, we measured the phenotypes induced by chimeras at

321   the FAMA stage in T1s and compared to those obtained for intact MKK5^{DD} and MKK7^{ED}. Expression

322   and subcellular localization of YFP-tagged MKKs was verified by confocal microscopy. We predicted

323   that certain domain combinations could result in non-functional chimeras. Because expression of

324   MKK5^{DD} and non-functional chimeras would give essentially the same phenotype at the FAMA stage (no

325   effect on stomatal development), it was important to discriminate MKK5^{DD}-like chimeras from non-

326   functional chimeras. We took two approaches to verify that kinases were still active. First, we measured

327   the intrinsic kinase activity against MPK3/6 in *in vitro* kinase assays (Supplemental Figure 2). Second, we

328   took advantage of the fact that both MKK5^{DD} and MKK7^{ED} drive robust inhibition of stomatal initiation at

329   the SPCH stage (Lampard et al., 2009) to create an *in vivo* assay for kinase activity. We expressed the

330   chimeras at the SPCH stage and quantified the degree of inhibition of stomatal initiation (Table 1).

331   To characterize the role of the N-terminus in MKK5, we replaced it with the N-terminus of

332   MKK7 (N7-MKK5^{DD}) and the chimera was expressed in FAMA stage cells. ~59% of T1 transformants

333   produced stomatal clusters (Figure 4B and G), though clusters were smaller than those generated by

334   MKK7^{ED}. In addition, 9% of T1 transformants showed inhibition of stomatal formation (Figure 4G). We

335   also noticed that N7-MKK5^{DD} partially relocalized to mitochondria (Figure 4B) similar to MKK7^{ED}

336   (Lampard et al., 2014). Our *in vitro* and *in vivo* controls for activity both indicated that N7-MKK5^{DD} was

337   less active than intact MKK5^{DD}; only ~27% of T1s inhibited stomatal initiation (Figure 4H) and *in vitro*

338   kinase activity was lower, especially towards MPK3 (Figure 4I). This dramatic output alteration

339   (aphenotypic MKK5^{DD} to a weak MKK7^{ED}-like behavior) suggests that the N-terminus is more than just a

340   structural/regulatory region required for protein activity. Instead, it appears to channel the MKK towards

341   specific phenotypic outcomes. This specificity behavior resembles that observed in yeast where MKKs

342   involved in other cellular processes were engineered to interact with components of the mating pathway,

343   but were only able to transduce a mating signal when their N-termini were replaced with the N-terminus

344   from Ste7, the mating specific MKK (Won et al., 2011).

345

346   **Figure 4: N-termini link MKKs to their phenotypic outputs and the C-terminal Loop B is required**

347   **for FAMA stage-specific regulation of MKK5.** (A-F) Paired micrographs of representative major

348   phenotype (left) and subcellular localization (right), of specific MKK5^{DD}- and MKK7^{ED}-YFP variants

349   (diagramed above). Black brackets mark clusters and asterisks indicate inhibition. YFP is in green and

350   cell outlines in magenta. For example, in (A) MKK5^{DD} expression results in a WT phenotype and the

351   protein is cytoplasmic and in (B) mitochondrial/cytoplasmic N7-MKK5^{DD} induces stomatal clustering.

352   Scale bars are 50 μm in phenotype images and 10 μm for localization images. (G) Quantification of

353   phenotypes in (A-F). (H) SPCH stage inhibition of lineage initiation. Error bars in (G) and (H) correspond

354   to 95% confidence interval. (I) *In vitro* kinase activity towards kinase inactive MPK3 and MPK6. Kinase

355   assays were performed in triplicates, normalized to unphosphorylated KI-MPK and averaged; error bars

356   represent standard errors.

357

358   If the N-terminus enforces MKK specific activities, then replacement of N7 by N5 in MKK7^{ED}

359   should reveal the endogenous response to MKK5 activation. With the N5-MKK7^{ED} chimera we found

360   efficient inhibition of lineage initiation at the SPCH stage and a normal ability to phosphorylate MPK3

361   and MPK6 *in vitro* (Figure 4H and I). Like MKK5^{DD} the chimera was cytoplasmic localized (compare A

362   and C in Figure 4). Unlike MKK5^{DD}, N5-MKK7^{ED} completely inhibited GC production (Figure 4C and

363   G). Thus, with this manipulation, we were finally able to recapitulate the stomatal lineage inhibition

364   phenotype we had expected from MKK5^{DD} based on its ability to inhibit stomatal development at earlier

365   stages (Lampard et al., 2009) and the loss of function stomatal cluster phenotype (Wang et al., 2007).

366

367   **Loop B prevents MKK5^{DD} from inhibiting stomata formation at the FAMA stage**

368   Demonstrating that development of FAMA-stage cells could be inhibited, however, raised the

369   question of why intact MKK5^{DD} is unable to do so. We hypothesized that sequences in the MKK5 C-

370   terminus act as negative regulatory regions. To test this idea, we first replaced the entire C-terminal

371   region of MKK5, creating MKK5^{DD}-C7. FAMA-stage expression did result in a partially penetrant

372   inhibition of stomatal formation where inhibited precursors coexisted with normal stomata (Figure 4D

373   and G). MKK5^{DD}-C7 displayed high activity in SPCH-stage lineage inhibition (Figure 4H), but was less

374   efficient than MKK5^{DD} in *in vitro* kinase assays, particularly towards MPK3 (Figure 4I). Because

375   previously reported MKK5 deletions in the CDR portion of the C-terminus did not significantly change

376   MKK5^{DD} activities (Lampard et al., 2014), we reasoned that putative regulatory regions were located in

377   the CPR.

378   The largest sequence differences between C5 and C7 reside in loop A and B in the CPR.

379   Substitution of loop A (MKK5^{DD}-7A) resulted in a chimera that did not affect stomatal development at

380   the FAMA stage (Figure 4E and G), but substitution of loop B (MKK5^{DD}-7B) led to inhibition of stomatal

381   formation at high frequency (Figure 4F and G). This result suggests that MKK5's loop B is a region that

382   blocks MKK5 from participating in stomatal inhibition at the FAMA stage. Interestingly, SPCH stage

383   activity was markedly reduced for both chimeras (Figure 4H), but *in vitro* activities of MKK5^{DD}-7A and

384   MKK5^{DD}-7B were at least as high as that of MKK5^{DD} (Figure 4I). These observations suggest that

385   MKK5^{DD}-7A and MKK5^{DD}-7B are catalytically active kinases but cannot generate appropriate signals *in*

386   *vivo*.

387

388   **Loop B is required for robust MKK7^{ED} activity**

389   If there was truly a discrete domain of MKK5 that was subject to negative regulation, then

390   transferring it to MKK7^{ED} should dampen the stomatal clustering phenotype at the FAMA stage (Figure

391   5A). We initially swapped the entire C-terminus, and the resulting MKK7^{ED}-C5 only produced normal

392   stomata, similarly to MKK5^{DD} (Figure 5B and G). This could suggest that C5 is able to block MKK7

393   inhibitory function at FAMA stage. However, monitoring other indicators of MKK activity (SPCH stage

394   lineage inhibition and *in vitro* phosphorylation of MPK3 and MPK6) suggested that C7 was essential for

395   overall activity (Figure 5H and I). Thus this phenotype is the result of creating a generally inactive MKK7

396   chimera, more than an effect due to the presence of MKK5 regulatory sequences. Thus, we split C5 into

397   CDR5 and CPR5, and determined if we could restore MKK7^{ED} activity *in vitro* and in the SPCH stage.

398   Activity was restored in MKK7^{ED}-CDR5: this chimera completely inhibited lineage initiation at the SPCH

399   stage and was indistinguishable from MKK7^{ED} in *in vitro* kinase assays (Figure 5H and I). Rather than

400   decreasing MKK7^{ED} function, however, MKK7^{ED}-C**D**R5 had a strikingly stronger inhibitory effect on

401   stomatal development at the FAMA stage than MKK7^{ED} (Figure 5C and G). In fact, it resembled the

402   strong phenotype produced by N5-MKK7^{ED} (Figure 4C). This implies that CDR5, like N5, channels

403   MKK activity to inhibition of stomatal development. In contrast, MKK7^{ED}-C**P**R5 was largely inactive at

404   both SPCH and FAMA stages (Figure 5D and G), and in *in vitro* phosphorylation assays against MPK3

405   and MPK6 (Figure 5H and I), indicating that CPR7 is necessary for MKK7^{ED} catalytic activity.

406

407   **Figure 5: Loops A and B are required for specific and robust FAMA stage MKK7 activities.** (A-F)

408   Paired micrographs of representative major phenotype (left) and subcellular localization (right), of

409   specific MKK7^{ED}-YFP variants diagramed above. Black brackets mark clusters and asterisks indicate

410   inhibition. YFP is in green and cell outlines in magenta; white arrowheads point to mitochondrial

411   localization. For example, in (A) MKK7^{ED} induces stomatal clustering (brackets) and is mitochondrial

412   localized (white arrowheads). Scale bars are 50 μm for phenotype images and 10 μm for localization

413   images. (G) Quantification of phenotypes in (A-F). (H) SPCH stage inhibition of lineage initiation. Error

414   bars in (G) and (H) correspond to 95% confidence interval. (I) *In vitro* kinase activity towards kinase

415   inactive MPK3 and MPK6. Kinase assays were performed in triplicates, normalized to unphosphorylated

416   KI-MPK and averaged; error bars represent standard errors.

417

418   So far, the domains from MKK5 that dampened MKK7^{ED} activity at the FAMA stage also

419   decreased the activity of the chimeras *in vitro* and at the SPCH stage (MKK7^{ED}-C5 and MKK7^{ED}-CPR5).

420   From these results, it appears that the CPR region is important for MKK7^{ED} catalytic activity and thus we

421   created smaller domain swaps (loops A and B) to attempt to transfer negative regulatory sequences from

422   MKK5 into MKK7^{ED} without affecting kinase functionality. MKK7^{ED}-5A and MKK7^{ED}-5B were active

423   *in vivo* (inhibited lineage initiation at the SPCH stage, Figure 5H) and *in vitro* (phosphorylated MPK3/6,

424   Figure 5I), although to different degrees. At the FAMA stage, MKK7^{ED}-5A inhibited stomatal formation

425   to a greater extent than MKK7^{ED} (Figure 5E and G). This behavior is similar to N5-MKK7^{ED} (Figure 4C)

426   and MKK7^{ED}-CDR5 (Figure 5C), suggesting that N5, loop 5A and CDR5 restrict MKK7^{ED} activity to

427   inhibition of stomatal development. In contrast, MKK7^{ED}-5B's ability to cause stomatal clustering and

428   inhibition of stomatal development at the FAMA stage was markedly reduced when compared to

429   MKK7^{ED} (Figure 5G). Because MKK7^{ED}-5B also showed reduced activities in other indicators of MKK

430   activity (Figure H and I), we concluded that the negative regulation of MKK5^{DD} is restricted to loop 5B

431   but cannot be transferred without affecting MKK7^{ED} catalytic activity. Nevertheless, the same results

432   highlight that loop 7B is required for robust MKK7^{ED} activity.

433

434   **Swapping domains allows specificity to be changed in MKK5^{DD} and MKK7^{ED}**

7

435   Our results show that the N-terminus, CPR region (loops A and B) and CDR region modulate

436   MKK activity. We showed that N7 and CPR7 are necessary for MKK7^{ED}-mediated GC clustering at the

437   FAMA stage, but when CDR5 is incorporated into MKK7^{ED}, GC production is inhibited. If our "wiring

438   diagram" for specificity is correct, then a chimera that contains the GC promoting domains from MKK7

439   but not the inhibitory CDR5 (i.e., N7-MKK5^{DD}-C7) should mimic MKK7^{ED}. Indeed, when we constructed

440   N7-MKK5^{DD}-C7, it resembled MKK7^{ED} both qualitatively and quantitatively (Figure 6A and C).

441   Likewise, N5-MKK7^{ED}-C5 should match MKK5^{DD} activities, and it does *in planta* (Figure 6B and C).

442   Interestingly, robust rewiring *in vivo* (Figure 6C and D) appears to be uncoupled from kinase activity *in*

443   *vitro*, as both rewired proteins were much less capable of phosphorylating MPK3 and MPK6 than

444   MKK5^{DD} and MKK7^{ED} (Figure 6E). One interpretation of these swaps is that specificity lies only outside

445   of the kinase domain. If this were true, then we should be able to generate a chimera that resembles N7-

446   MKK5^{DD}-C7 and MKK7^{ED} using the kinase domain from another MKK. We selected the kinase domain

447   of MKK6 that can also phosphorylate MPK3 and MPK6 *in vitro* (Popescu et al., 2009), and created N7-

448   MKK6^{DD}-C7. Expression of N7-MKK6^{DD}-C7 at the FAMA stage, however, did not produce any

449   noticeable phenotype (Supplemental Figure 6). This suggests that although kinase domains in MKK5 and

450   MKK7 are not differential, they still contain stomatal fate-enabling regions.

451

452   **Figure 6: MKK5 and MKK7 activity and localization in the stomatal lineage can be reciprocally**

453   **rewired.** (A-B) paired micrographs of representative major phenotype (left) and subcellular localization

454   (right), specific MKK-YFP variants diagramed above. Black brackets mark clusters; YFP is in green and

455   cell outlines in magenta; white arrowheads point to mitochondrial localization. (A) N7-MKK5^{DD}-C7

456   mimics MKK7^{ED} in that it produces clusters and can localize to mitochondria. (B) N5-MKK7^{ED}-C5

457   mimics MKK5^{DD} in that it has a WT phenotype and localizes in the cytoplasm. Scale bars are 50 μm in

458   phenotype images and 10 μm for localization images. (C) Quantification of phenotypes (A-B). (D) SPCH

459   stage inhibition of lineage initiation. Error bars in (C) and (D) correspond to 95% confidence interval. (E)

460   *In vitro* kinase activity towards kinase inactive MPK3 and MPK6. Kinase assays were performed in

461   triplicates, normalized to unphosphorylated KI-MPK and averaged; error bars represent standard errors.

462

463   **Comprehensive analysis of chimeras reveals functions of MKK domains**

464   We repeatedly observed that the ability of native and chimeric MKKs to phosphorylate their

465   targets *in vitro* does not predict their activities *in vivo*. In fact, when chimera data are considered together,

466   *in vitro* versus *in vivo* data have no statistical correlation (Supplemental Figure 7). In contrast, when only

467   *in vivo* data were compared, activities in SPCH and FAMA stages were positively correlated (Figure 7A).

468   Interestingly, native and chimeric MKKs were distributed in two subpopulations. MKKs closer to the

469   regression line promoted stomatal clustering (red dots) or inhibited stomatal formation (black dots).

470   MKKs further from the regression line had no effect in stomatal development at the FAMA stage (blue

471   dots), but had a broad range of activities at the SPCH stage (shaded area in Figure 7A). This behavior

472   might be reflecting the additional regulation that some of the MKKs showed at the FAMA stage.

473

474   **Figure 7: MKK5 defines a cluster of chimeras with low activity at FAMA stage, whereas clustering**

475   **and inhibiting chimeras group in two independent clusters.** (A) SPCH and FAMA stage activities

476   show a weak positive correlation. Shaded area corresponds to activities at the FAMA stage lower than

477   30%. Data points are colored according to the cluster they belong to in (B). MKK activities at the FAMA

478   stage are separated into three clusters (B): cluster 1 contains MKKs that show no phenotypic effect and

479   contain loop 5B; cluster 2 contains MKKs that lead to stomatal clustering and contain N7; and, cluster 3

480   contains MKKs that lead to inhibition of stomatal development and contain loop 7B. Numbers next to

481   nodes correspond to approximately unbiased *p*-values with bootstrap replications set to 1000. Chimeras

482   not significantly different in Chi-squared tests if independence are indicated with an identical number (p >

483   0.05).

484

485   We reasoned that MKKs subject to the same regulation would share structural similarities. To test

486   this hypothesis and generate an overall picture of the relationship between MKK structural domains and

487   *in vivo* functions, we clustered 15 native and chimeric MKKs and controls according to their quantitative

488   phenotype data at the FAMA stage (clustering detailed in methods). Constructs robustly fell into three

489   clusters (Figure 7B): Cluster 1, no phenotypic effect; Cluster 2, induces stomatal proliferation; and

490   Cluster 3, inhibits stomatal formation (the presumed endogenous role for MKK5). Within clusters,

491   however, not all MKKs were identical. We performed sequential tests of independence to determine how

492   similar the distribution of phenotype frequencies was between chimeras in each cluster. Cluster 1 was

493   composed of MKKs similar to MKK5^{DD} (group 1) and MKKs similar to inactive YFP (group 2). Cluster 2

494   was statistically separated into weak MKK7^{ED}-like chimeras (group 3) and two MKKs that induced strong

495   clustering, yet were different from each other. Cluster 3 was statistically separated into strong inhibitors

496   of stomatal formation (group 4) and weak inhibitors (different from each other).

497   To summarize, when analyzing native and chimeric MKK structures across Clusters, we see that

498   loops A and B have discrete functions in selecting MKK-specific outputs and in kinase activity *in vivo*.

499   Loop A can be thought of as a "channel selector", that, together with N-terminus and CDR, selects

500   between the normal role of arresting stomatal progression and the artificial role of promoting stomatal

501   clustering. Loop B is a "volume control" with the 7B version increasing, and 5B decreasing, the

502   phenotypes specified by the other domains of the MKKs

503

504   **MPK6 mediates GC inhibition, but like MKK5, is prevented from doing so at the FAMA stage.**

505   Previous loss- and gain-of-function experiments placed MPK3 and MPK6 downstream of an

506   activated MKK4/5 homologue (NtMEK2), suppressing stomatal formation (Wang et al., 2007) in the

507   early stages of the stomatal lineage, but this assay could not address the potential for MPK3 and MPK6 to

508   mediate FAMA-stage activities. Our chimeras that drive stomatal inhibition at the FAMA-stage, however,

509   could be used to see whether either mediated such late stage inhibition. We used N5-MKK7^{ED} which, in

510   WT led to complete inhibition of stomatal development (Fig 8C, Table 1). When expressed in the loss of

10

511   function *mpk6-3* background, N5-MKK7^{ED} failed to promote complete inhibition in 19 independent T1s

512   (Figure 8D) indicating that MPK6 is likely downstream. This led us to the question of whether MPK6,

513   like MKK5^{DD}, would also be actively inhibited from effecting fate at the FAMA stage. To test this, we

514   created a constitutively active MPK6 (MPK6^{DE}) (Berriri et al., 2012) and tested its ability to suppress

515   stomatal formation. Expression of MPK6^{DE} (but not MPK3^{DE}, Figure 8A, Table 1), inhibited stomatal

516   progression at the SPCH stage, indicating that MPK6^{DE} is active in this assay. When expressed at the

517   FAMA stage, however, MPK6^{DE} did not affect stomatal development (Figure 8B, Table 1), a phenotypic

518   output remarkably similar to that of MKK5^{DD} (early, but not late, inhibition). We hypothesized that

519   MKK5 and MPK6 normally repress stomatal development, but are actively prevented from having this

520   effect at the FAMA stage.

521

522   **Figure 8: MPK6 inhibits stomatal development at the FAMA stage in a MKK-specific manner.** (A

523   and B) Micrographs indicating the requirement for MPK6 as a downstream factor in N5-MKK7^{ED}-

524   mediated FAMA-stage inhibition (asterisks). In *mpk6* mutants (B), stomata (arrowhead) coexist with

525   precursors that exit the lineage. (C-and D) DIC micrographs showing results of expression of MPK6^{DE} at

526   SPCH and FAMA stages, stomata are highlighted in green. MPK3^{DE} does not affect development at any

527   stage (Table 1). Scale bars in are 50 μm.

528

529

530   **Discussion**

531   In multicellular organisms, coordinated development requires constant communication between

532   cells and the evaluation of environmental conditions. All this information is integrated to decide from a

533   spectrum of possible outputs, and the spectrum is frequently limited by a cell's identity. In previous, more

534   superficial studies, FAMA stage cells appeared to lose the ability to inhibit stomatal development upon

535   MAPK activation (Lampard et al., 2009). Here we show that these cells do not lack the capacity to be

536   inhibited, but rather that MKK5 (and possibly MPK6) may be actively prevented from participating in

537   this cellular outcome. Structural analysis and engineered chimeras revealed that this regulation and other

538   specific responses rely on distinct MKK domains.

539   We found that Arabidopsis MKKs behave as modular proteins with four discrete regions: N-

540   terminus, CDR and two loops (A and B) in the CPR. N-termini contribute to subcellular localization

541   (Figure 4 and in (Lampard et al., 2014)), to phenotypic output (Figure 4) and may mediate interactions

542   with downstream MPKs through their docking domains. In particular, we hypothesize that N7 has the

543   ability to bind different types of MPK. Throughout development, MKK7 inhibits stomatal development

544   by recruiting MPK3/6, but a yet unknown proliferative MPK mediates stomatal clustering at the FAMA

545   stage (Figure 9A). In the C-termini, Arabidopsis MKKs 1, 2, 4, 5 and 6 contain an extension that could be

546   equivalent to the MKKK-interacting domain for versatile docking (DVD) in human MEKs 1, 3, 4, 6 and 7

547   (Supplemental Figure 4) (Takekawa et al., 2005). Arabidopsis MKK7, 8, 9, and 10, however, lack this

548   domain, making it unclear how they engage the appropriate MKKK. In fact, the addition of CDR5 to

549   MKK7^{ED} restricted this kinase's activity to an inhibitory output (Figure 5C and G), suggesting that CDR5

550   interferes with MKK7^{ED} interactions. Upstream of the CDR, Loop A and B are two surface-exposed

551   modules in the CPR that may contribute to establishing interactions with other network components. In

552   our experiments, swapping loop A in MKK7^{ED} restricted its phenotypic output such that MKK7^{ED}-5A

553   only inhibited stomata formation (Figure 5E, G).We propose then, that loop A promotes certain MKK-

554   MPK interactions or, alternatively, restricts how MPKs contact MKKs. This hypothesis is supported by

555   sequence similarities between human MEKs that share the same downstream MAPKs (Keshet and Seger,

556   2010). For example, ERK kinases MEK1 and MEK2 have identical loop As, and p38 kinases MEK3 and

557   MEK6 differ at only one site (Supplemental Figure 4). Interestingly, human MEK7, which can

558   phosphorylate both JNK and p38, shares some residues with MEK3 and MEK6 and others with the JNK

559   kinase MEK4.

560   The function of loop B seems to be associated to MKK-specific regulation. Our data shows that

561   loop B is required for robust MKK7^{ED} activity, but it prevents MKK5^{DD}-mediated inhibition at the FAMA

562   stage (Figure 4F-G and 5F-G). Based on these phenotypes, we propose that loop B mediates interactions

12

563   with different scaffolds (Figure 9). A signal-promoting scaffold binds loop 7B and enforces MKK7

564   interactions with its cognate MKKK and MPK (Figure 9A). Such a scaffold would also explain why *in*

565   *vivo* activity of MKK7^{ED} was always stronger than that of MKK5^{DD}, even though *in vitro* assays showed

566   an opposite pattern. On the other hand, we predict that a distinct scaffold recruited by loop 5B prevents

567   MKK5^{DD} from inhibiting stomatal development at the FAMA stage (inhibitory scaffold) (Figure 9B).

568   This prediction could also partially explain the behavior of certain chimeras. For example, the inhibitory

569   scaffold would bind MKK7^{ED}-5B through loop 5B and dampen MKK7^{ED} activities. Likewise, a signal-

570   promoting scaffold would bind MKK5^{DD}-7B through loop 7B, releasing the inhibition of MKK5^{DD}.

571

572   **Figure 9: A new model derived from activities during stomatal development for the endogenous**

573   **MKK5 pathway and another activated by MKK7.** (A) In the MKK7 pathway, MKK7 mimics MKK5

574   in early development, forcing precursors to exit the stomatal lineage. At the last stage, MKK7 induces

575   two phenotypes. Firstly, MKK7 induces stomatal clustering by means of an unknown MKK7-specific

576   MPK (orange circle). This proliferation depends on MKK7 mitochondrial localization (Lampard et al.,

577   2014). Secondly, MKK7 forces precursors to exit the lineage by escaping MKK5-specific regulation. An

578   MKK7 scaffold enforces interactions between MKK7 and other components (MPKs and YODA, gray

579   circles) within the network. (B) In the endogenous pathway, MKK5 and MPK3/6 (black circles) are

580   involved in transducing developmental signals that inhibit stomatal lineage initiation and GMC

581   commitment, and initiating defense and stress responses. At the last stage of development, a stage-

582   specific MKK5 scaffold prevents MKK5 (and possibly MPK3/6) from inhibiting stomatal formation, only

583   allowing defense and stress responses.

584

585   The existence of signal-enhancing and inhibiting MAPK scaffolds in plants is supported by recent

586   findings (Zhao et al., 2014; Cheng et al., 2015; Zhang et al., 2015). While the relevance of the first type is

587   quite intuitive, the second type is more controversial. The inhibitory scaffold EDR1 was identified in the

588   context of pathogen defense. Current hypotheses are that EDR1 provides a failsafe against inadvertently

589   activating defense or cell death programs when other (not pathogen-induced) cues activate MAPK

590   signaling. EDR modulates MPK3 activity indirectly by interacting with MKK4/5 and regulating their

591   abundance (Zhao et al., 2014). Interestingly, we observed in FAMA stage cells that MPK6 was only

592   inhibited when the upstream MKK was also inhibited. The clearest evidence that MKK5-MPK3/6 are

593   scaffolded in FAMA stage cells would be, of course, to identify the scaffold. We tested whether EDR1

594   worked to inhibit FAMA-stage expressed MKK5^{DD}, however we failed to see a loss of inhibition in *edr1*

595   (none seen in 20 independent T1s). EDR1 is a member of the large Raf-like MKKKs family (Ichimura et

596   al., 2002) and potentially any of the 48 members of this family (alone or in combination) could serve as a

597   stomatal scaffold. As testing the entire family in not technically feasible, we used stomatal lineage

598   expression data (Adrian et al., 2015) to identify two close homologues of EDR1 expressed at the FAMA

599   stage, MAP3Kδ1 (At1g11850) and MAP3Kδ5 (At4g24480). *MAP3Kδ1* and *MAP3Kδ5* mutants, however,

600   were indistinguishable from WT in their response to FAMA stage MKK5^{DD} expression (0/20 independent

601   T1s for each). Thus, the molecular identity of the stomatal scaffold remains of great future interest.

602   MKK4/5 face the problem of being used in early stages to repress stomatal progression, but being

603   required for physiological regulation in guard cells. At the FAMA stage, MKK4/5 must therefore be

604   actively rerouted from their previous role inhibiting stomatal development to allow terminal

605   differentiation of guard cells (Figure 9). A negative scaffold acting late in the stomatal lineage to redirect

606   MKK4/5 would provide an elegant solution to a complex signal integration problem.

607

608

609 **References**

610

611 **Adrian, J. et al.** (2015). Transcriptome Dynamics of the Stomatal Lineage: Birth, Amplification, and

612   Termination of a Self-Renewing Population. Dev. Cell **33**: 107–118.

613 **Andreasson, E. and Ellis, B.** (2010). Convergence and specificity in the Arabidopsis MAPK nexus.

614   Trends Plant Sci. **15**: 106–113.

615 **Bao, M.Z., Schwartz, M.A., Cantin, G.T., Yates, J.R., and Madhani, H.D.** (2004). Pheromone-

616   Dependent Destruction of the Tec1 Transcription Factor Is Required for MAP Kinase Signaling

617   Specificity in Yeast. Cell **119**: 991–1000.

618 **Bergmann, D.C., Lukowitz, W., and Somerville, C.R.** (2004). Stomatal Development and Pattern

619   Controlled by a MAPKK Kinase. Science (80-.). **304**: 1494 LP-1497.

620 **Berriri, S., Garcia, a. V., Frei dit Frey, N., Rozhon, W., Pateyron, S., Leonhardt, N., Montillet, J.-**

621   **L., Leung, J., Hirt, H., and Colcombet, J.** (2012). Constitutively Active Mitogen-Activated

622   Protein Kinase Versions Reveal Functions of Arabidopsis MPK4 in Pathogen Defense Signaling.

623   Plant Cell **24**: 1–14.

624 **Brennan, D.F., Dar, A.C., Hertz, N.T., Chao, W.C.H., Burlingame, A.L., Shokat, K.M., and Barford,**

625   **D.** (2011). A Raf-induced allosteric transition of KSR stimulates phosphorylation of MEK. Nature

626   **472**: 366–369.

627 **Brückner, S., Köhler, T., Braus, G.H., Heise, B., Bolte, M., and Mösch, H.-U.** (2004). Differential

628   regulation of Tec1 by Fus3 and Kss1 confers signaling specificity in yeast development. Curr. Genet.

629   **46**: 331–342.

630 **Chen, R.E. and Thorner, J.** (2007). Function and regulation in MAPK signaling pathways: Lessons

631   learned from the yeast Saccharomyces cerevisiae. Biochim. Biophys. Acta - Mol. Cell Res. **1773**:

632   1311–1340.

633 **Cheng, Z., Li, J.-F., Niu, Y., Zhang, X.-C., Woody, O.Z., Xiong, Y., Djonovic, S., Millet, Y., Bush, J.,**

634   **McConkey, B.J., Sheen, J., and Ausubel, F.M.** (2015). Pathogen-secreted proteases activate a

635   novel plant immune pathway. Nature **521**: 213–216.

636   **Chou, S., Huang, L., and Liu, H.** (2004). Fus3-Regulated Tec1 Degradation through SCFCdc4

637   Determines MAPK Signaling Specificity during Mating in Yeast. Cell **119**: 981–990.

638   **Dóczi, R., Ökrész, L., Romero, A.E., Paccanaro, A., and Bögre, L.** (2012). Exploring the evolutionary

639   path of plant MAPK networks. Trends Plant Sci. **17**: 518–525.

640   **Goldsmith, E.J., Akella, R., Min, X., Zhou, T., and Humphreys, J.M.** (2007). Substrate and docking

641   interactions in serine/threonine protein kinases. Chem. Rev. **107**: 5065–5081.

642   **Good, M.C., Zalatan, J.G., and Lim, W.A.** (2011). Scaffold Proteins: Hubs for Controlling the Flow of

643   Cellular Information. Science (80-.). **332**: 680–686.

644   **Guex, N. and Peitsch, M.C.** (1997). SWISS-MODEL and the Swiss-Pdb Viewer: An environment for

645   comparative protein modeling. Electrophoresis **18**: 2714–2723.

646   **Hanks, S.K. and Hunter, T.** (1995). Protein kinases 6. The eukaryotic protein kinase superfamily: kinase

647   (catalytic) domain structure and classification. FASEB J. **9**: 576–596.

648   **Ichimura, K. et al.** (2002). Mitogen-activated protein kinase cascades in plants: a new nomenclature.

649   Trends Plant Sci **7**: 301–308.

650   **Jia, W. et al.** (2016). Mitogen-Activated Protein Kinase Cascade MKK7-MPK6 Plays Important Roles in

651   Plant Development and Regulates Shoot Branching by Phosphorylating PIN1 in Arabidopsis. PLOS

652   Biol. **14**: e1002550.

653   **Kannan, N. and Neuwald, A.F.** (2004). Evolutionary constraints associated with functional specificity

654   of the CMGC protein kinases MAPK ,.: 2059–2077.

655   **Keshet, Y. and Seger, R.** (2010). The MAP Kinase Signaling Cascades: A System of Hundreds of

656   Components Regulates a Diverse Array of Physiological Functions. In MAP Kinase Signaling

657   Protocols: Second Edition, R. Seger, ed (Humana Press: Totowa, NJ), pp. 3–38.

658   **Knight, J.D.R., Qian, B., Baker, D., and Kothary, R.** (2007). Conservation, variability and the

659   modeling of active protein kinases. PLoS One **2**.

660   **Lampard, G.R., Lukowitz, W., Ellis, B.E., and Bergmann, D.C.** (2009). Novel and Expanded Roles

661   for MAPK Signaling in Arabidopsis Stomatal Cell Fate Revealed by Cell Type – Specific

662   Manipulations. **21**: 3506–3517.

663   **Lampard, G.R., Macalister, C.A., and Bergmann, D.C.** (2008). Is Controlled by MAPK-Mediated

664   Regulation of the bHLH SPEECHLESS. **322**: 1113–1116.

665   **Lampard, G.R., Wengier, D.L., and Bergmann, D.C.** (2014). Manipulation of mitogen-activated

666   protein kinase kinase signaling in the Arabidopsis stomatal lineage reveals motifs that contribute to

667   protein localization and signaling specificity. Plant Cell **26**: 3358–71.

668   **Macalister, C.A., Ohashi-ito, K., and Bergmann, D.C.** (2007). Transcription factor control of

669   asymmetric cell divisions that establish the stomatal lineage. **445**: 537–540.

670   **McKay, M.M., Ritt, D. a, and Morrison, D.K.** (2009). Signaling dynamics of the KSR1 scaffold

671   complex. Proc. Natl. Acad. Sci. U. S. A. **106**: 11022–7.

672   **Müller, J., Beck, M., Mettbach, U., Komis, G., Hause, G., Menzel, D., and Šamaj, J.** (2010).

673   Arabidopsis MPK6 is involved in cell division plane control during early root development, and

674   localizes to the pre-prophase band, phragmoplast, trans-Golgi network and plasma membrane. Plant

675   J. **61**: 234–248.

676   **Murphy, L.O. and Blenis, J.** (2006). MAPK signal specificity: the right place at the right time. Trends

677   Biochem. Sci. **31**: 268–275.

678   **Murphy, L.O., Smith, S., Chen, R., Fingar, D.C., and Blenis, J.** (2003). Molecular interpretation of

679   ERK signal duration by immediate early gene products. **4**.

680   **Nakagawa, T., Nakamura, S., Tanaka, K., Kawamukai, M., Suzuki, T., Nakamura, K., Kimura, T.,**

681   **and Ishiguro, S.** (2008). Development of R4 Gateway Binary Vectors (R4pGWB) Enabling High-

682   Throughput Promoter Swapping for Plant Research. Biosci. Biotechnol. Biochem. **72**: 624–629.

683   **Ohashi-ito, K. and Bergmann, D.C.** (2006). Arabidopsis FAMA Controls the Final Proliferation /

684   Differentiation Switch during Stomatal Development. **18**: 2493–2505.

685   **Popescu, S.C., Popescu, G. V, Snyder, M., and Dinesh-kumar, S.P.** (2009). Integrated analysis of co-

686   expressed MAP kinase substrates in Arabidopsis thaliana. **4**: 524–527.

687   **Raman, M., Chen, W., and Cobb, M.H.** (2007). Differential regulation and properties of MAPKs.

688   Oncogene **26**: 3100–3112.

689   **Rodriguez, M.C.S., Petersen, M., and Mundy, J.** (2010). Mitogen-Activated Protein Kinase Signaling

690   in Plants. Annu. Rev. Plant Biol. **61**: 621–649.

691   **Schaeffer, H.J., Catling, A.D., Eblen, S.T., Collier, L.S., Krauss, A., and Weber, M.J.** (1998). MP1:

692   A MEK Binding Partner That Enhances Enzymatic Activation of the MAP Kinase Cascade. Science

693   (80-.). **281**: 1668 LP-1671.

694   **Sievers, F., Wilm, A., Dineen, D., Gibson, T.J., Karplus, K., Li, W., Lopez, R., McWilliam, H.,**

695   **Remmert, M., Söding, J., Thompson, J.D., and Higgins, D.G.** (2011). Fast, scalable generation of

696   high-quality protein multiple sequence alignments using Clustal Omega. Mol. Syst. Biol. **7**.

697   **Takekawa, M., Tatebayashi, K., and Saito, H.** (2005). Conserved docking site is essential for activation

698   of mammalian MAP kinase kinases by specific MAP kinase kinase kinases. Mol. Cell **18**: 295–306.

699   **Teis, D., Wunderlich, W., and Huber, L.A.** (2002). Localization of the MP1-MAPK scaffold complex

700   to endosomes is mediated by p14 and required for signal transduction. Dev. Cell **3**: 803–814.

701   **Wang, H., Ngwenyama, N., Liu, Y., Walker, J.C., and Zhang, S.** (2007). Stomatal Development and

702   Patterning Are Regulated by Environmentally Responsive Mitogen-Activated Protein Kinases in

703   Arabidopsis. **19**: 63–73.

704   **Wang, W., Barnaby, J.Y., Tada, Y., Li, H., Tör, M., Caldelari, D., Lee, D., Fu, X.-D., and Dong, X.**

705   (2011). Timing of plant immune responses by a central circadian regulator. Nature **470**: 110–114.

706   **Won, A.P., Garbarino, J.E., and Lim, W. a** (2011). Recruitment interactions can override catalytic

707   interactions in determining the functional identity of a protein kinase. Proc. Natl. Acad. Sci. U. S. A.

708   **108**: 9809–9814.

709   **Yang, S.H., Sharrocks, A.D., and Whitmarsh, A.J.** (2013). MAP kinase signalling cascades and

710   transcriptional regulation. Gene **513**: 1–13.

711   **Zhang, Y.** (2008). I-TASSER server for protein 3D structure prediction. BMC Bioinformatics **9**: 40.

712   **Zhang, Y., Wang, P., Shao, W., Zhu, J.-K., and Dong, J.** (2015). The {BASL} Polarity Protein

713   Controls a {MAPK} Signaling Feedback Loop in Asymmetric Cell Division. Dev. Cell **33**: 136–149.

714   **Zhao, C., Nie, H., Shen, Q., Zhang, S., Lukowitz, W., and Tang, D.** (2014). EDR1 Physically Interacts

715   with MKK4/MKK5 and Negatively Regulates a MAP Kinase Cascade to Modulate Plant Innate

716   Immunity. PLoS Genet. **10**.

717

718   **Supplemental Figure legends**

719

720   **Supplemental Figure 1: Yeast two-hybrid assay with native and chimeric MKKs and MPK3/MPK6.**

721   Representative yeast two-hybrid assay between MKK chimeras and MPK3/6 at 3 days of growth on

722   control (-LW) and interaction (-LWH); three patches are serial (10 fold) dilutions.

723

724   **Supplemental Figure 2:** *In vitro* **kinase assays of MKKs and chimeras using kinase inactive (KI)**

725   **MPK3 and MPK6 as substrates.** Phosphorylation assays were performed as described in methods.

726   Samples were separated in SDS-PAGE, transferred to PVDF membranes and probed with anti-pERK

727   antibody. Western blots were quantified and average of experiments was used as an estimation of *in vitro*

728   activity. Each lane is labeled with the figure where the data is presented (grey bar marked *Figures*), the

729   kinase used with a graphic representation and with its full name in bottom panel. Samples unassigned to

730   any figure (labeled as "-" in *Figure*) were not presented in the main figures of this manuscript for the sake

731   of brevity, but are included here to allow us to keep the blots intact. Red squares highlight samples that

732   were not considered for quantification due to detection artifacts.

733

734   **Supplemental Figure 3: Multiple sequence alignment** (Sievers et al., 2011) **of catalytic domains in**

735   **MPK kinases from mouse, rat, human and *Arabidopsis thaliana*.** A, Conserved subdomains (**Subdom.**)

736   and consensus sequences (**Consen.**) are represented on top of the alignment and follow the same codes

737   and convention for an alignment of 60 different kinases by Hanks and Hunter (Hanks and Hunter, 1995).

738   In the consensus line: *uppercase letters*, invariant residues; *lowercase residues*, nearly invariant residues;

739   *o*, positions conserving nonpolar residues; *, positions conserving polar residues; +, positions conserving

740   small residues with near neutral polarity. Mammalian representative kinases selected for the alignment

741   have been crystalized and belong to **AGC group** [cAMP-dependent kinase, cGMP-dependent kinase,

742   etc.], **CAMK group** [Calcium-calmoduline-dependent protein kinase], **CMGC group** [cyclin-dependent

743   kinase, mitogen-activated kinase, glycogen synthase kinase and cyclin-dependent-like kinase] and **STE**

744 **group** [homologues of STE11 and STE20]. Gray boxes show CMGC insert (Goldsmith et al., 2007) in

745 ERK2, CDK2 and p38, and Pro-rich sequence (PRS, involved in binding the scaffold MP1) in MEK1 and

746 MEK2 were included in the alignment and cause an expansion of subdomain X. Secondary structure (**2°**

747 **str.**) information is overlaid in the alignment (red for α-helices and yellow for β-strands). Conserved α-

748 helices and β-strands are labeled following convention (Hanks and Hunter, 1995; Knight et al., 2007).

749 Due to CMGC insert and PRS, αG helix is located in two different regions of the alignment and was

750 named differently (residues underlined): **αG1** for MmPKA, HsARK-1, RnCaMKI, RnERK2, HsCDK2

751 and Hsp38; and **αG2** for HsMEK1/2 and AtMKK5/7. In green text, missing residues in crystal structures

752 from HsMEK1 and HsMEK2 which include the PRS. B, Table provides general information and

753 structural model names for kinases used in this comparison. C, Multiple sequence alignment of N- and C-

754 termini from human MEK1/2 and Arabidopsis MKK5/7. Sequences highlighted in gray correspond to

755 first and last three amino acids of the catalytic domains shown in A.

756

757 **Supplemental Figure 4: Multiple sequence alignment of C-termini in Arabidopsis and human**

758 **MKKs.** Top panel, partial sequences for all Arabidopsis and human MKKs were aligned with

759 ClustalOmega. Loops A and B defined for Arabidopsis MKKs are highlighted in gray. Number of first

760 amino acid of the partial sequence is noted to the left of each sequence. The long C-terminal extension of

761 AtMKK3 is truncated in this figure. Bottom panel, genes used in the alignment. Name of genes for

762 Arabidopsis correspond to Arabidopsis Genome Initiative (AGI) codes and GeneCards (GC) for humans.

763 NCBI GI, National Center for Biotechnology Information protein sequence identifier.

764

765 **Supplemental Figure 5: Multiple sequence alignment for MKK4, MKK5, MKK7 and MKK9.**

766 Domains described in (Lampard et al., 2014) are highlighted in blue and green.

767

768 **Supplemental Figure 6: Representative phenotype and subcellular localization of transgenic**

769 **seedlings expressing FAMAp:N7-MKK6^{EE}-C7.**

770

771   **Supplemental Figure 7:** *In vitro* **kinase activity of MKKs does not correlate with their** *in vivo*

772   **activity**. Linear regressions for MPK3 or MPK6 activity versus SPCH stage (A) or FAMA stage (B)

773   activities, with their formulas and R^2, are displayed in the figure. FAMA stage activity was calculated as

774   the addition of phenotypes different than normal (Inhibited, Small and Large clusters in Table 1).

Figure 1

A Early Development

MKKK

MKK

MPK

SPCH Stage

MUTE Stage

MMC

M
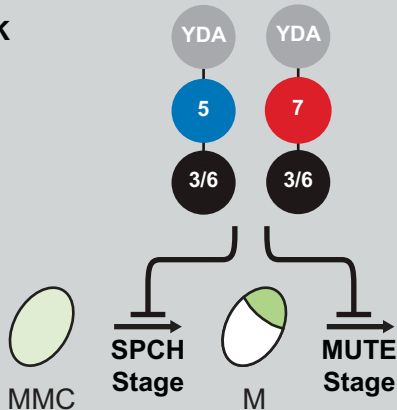
B Late Development

MKKK

MKK

MPK

FAMA Stage

GMC

GC

MKK5DD
MKK7ED

C
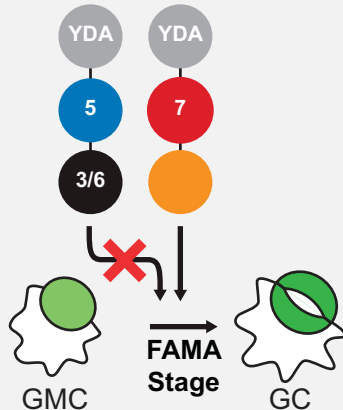
D
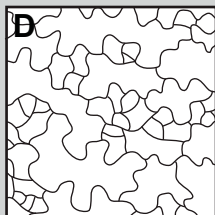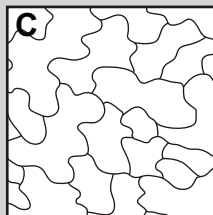
Common Outputs

MKK5DD

MKK7ED

E

F
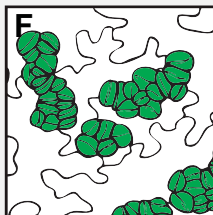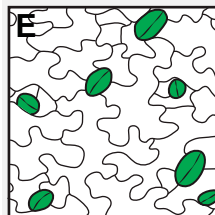
Divergent Outputs

Figure 2

A

Phenotypes due to FAMA stage expression

Inhibited	Normal	Clusters	
		Small	Large

B

■ YFP ■ MKK5^{DD} ■ MKK7^{ED}

Figure 3

A

N-terminus   C-terminus

MKK5^{DD}

A B

CPR

CDR

Catalytic core

B

N-terminus

5A

αG

5B

αF

αA

C-terminus

C

N-terminus   C-terminus

MKK7^{ED}

A B

CPR

CDR

Catalytic core

D

7A

αG

N-terminus

7B

αF

αA

C-terminus

Figure 4

Figure 5

Figure 6

MKK5^{DD}

MKK7^{ED}

C

D
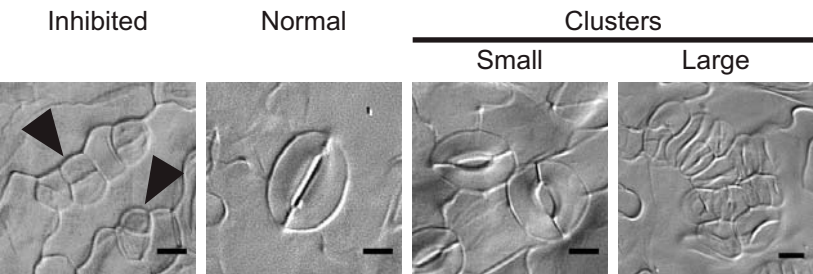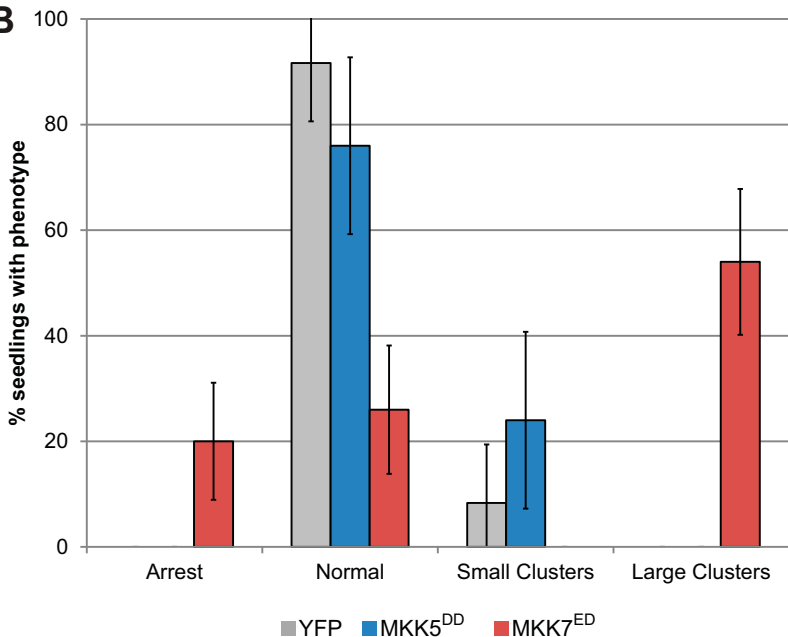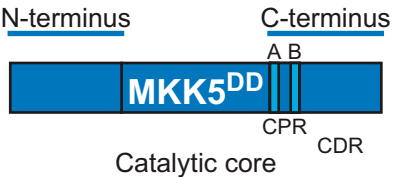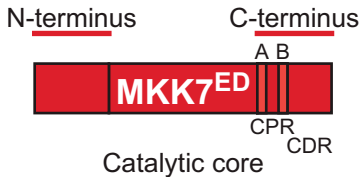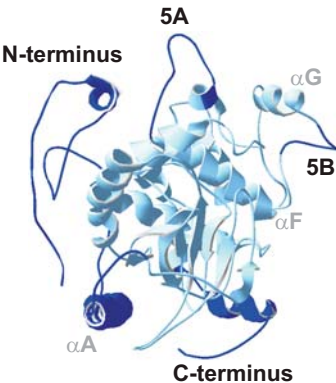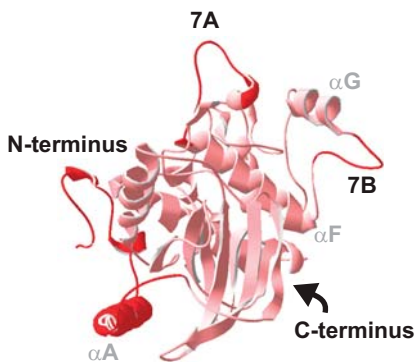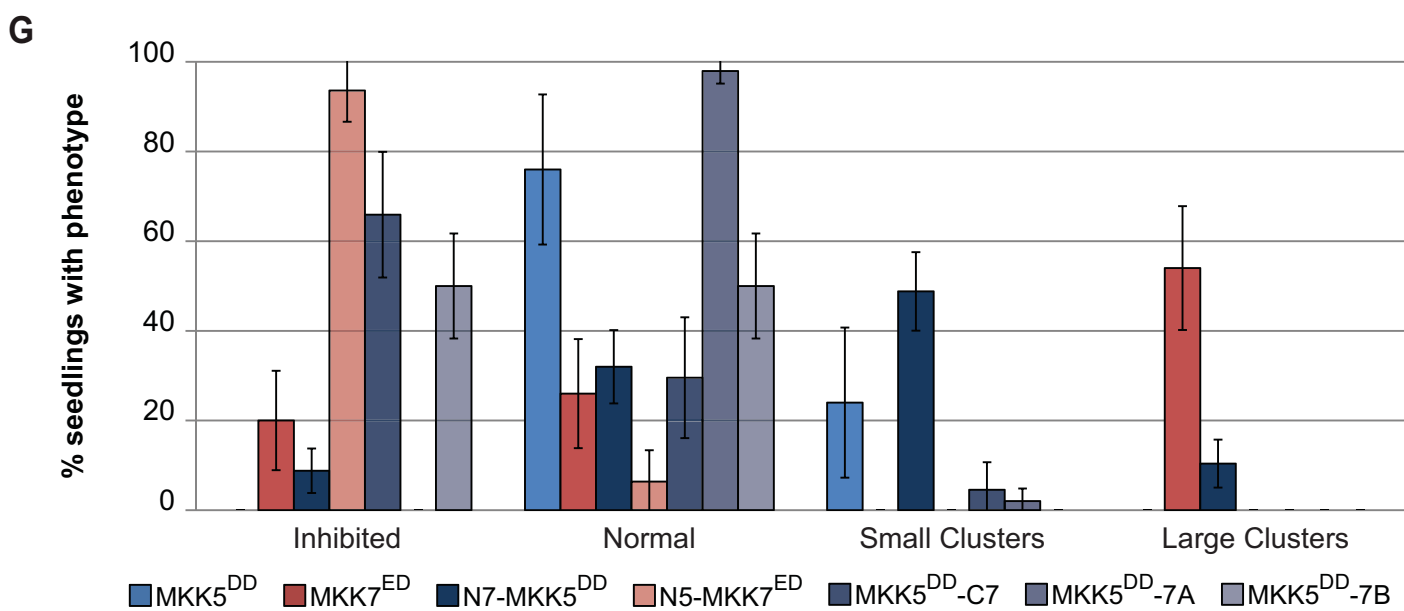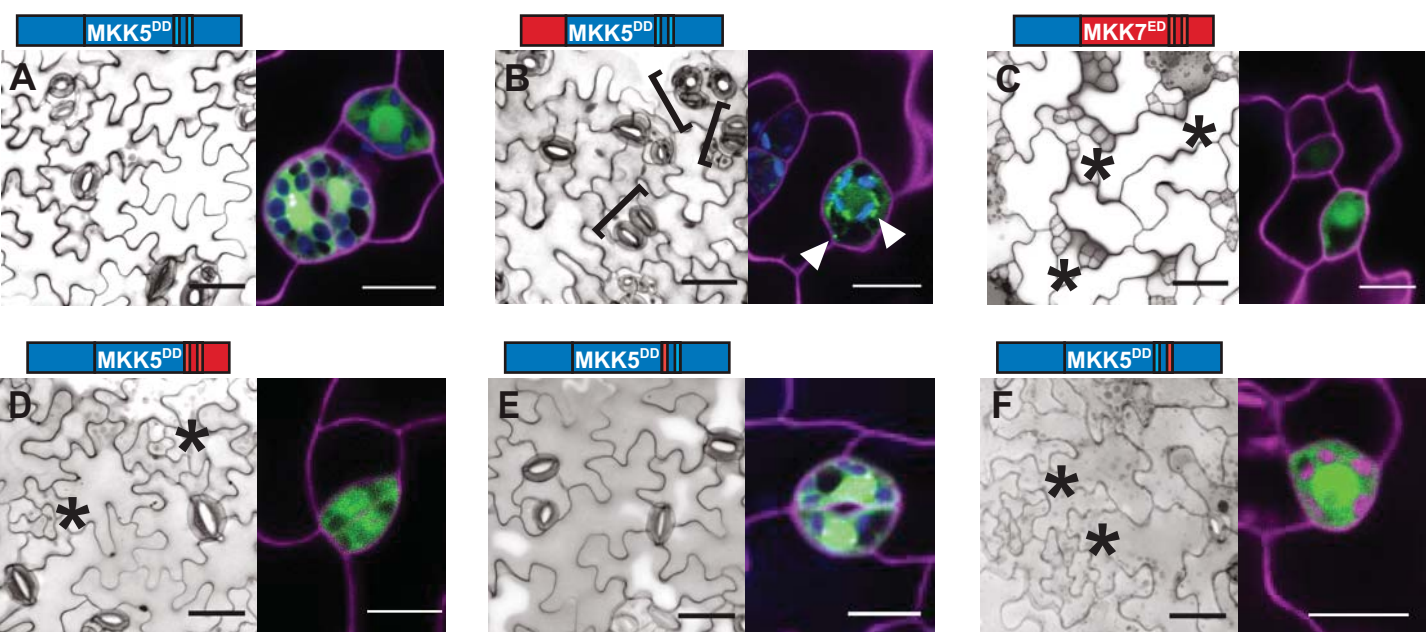
% seedlings showing inhibition at SPCH stage

E
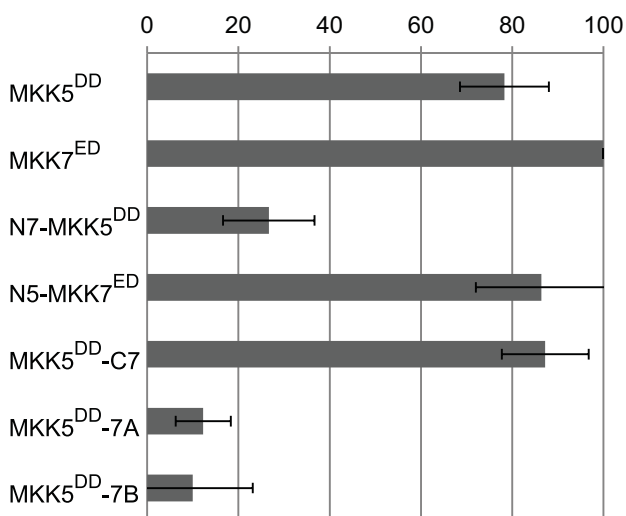
Relative Kinase Activity

Figure 7

A

y = 0.56x + 24.75
R² = 0.4206

B
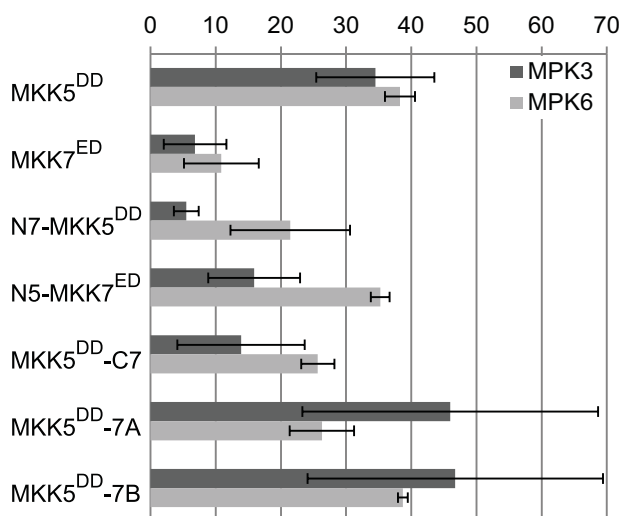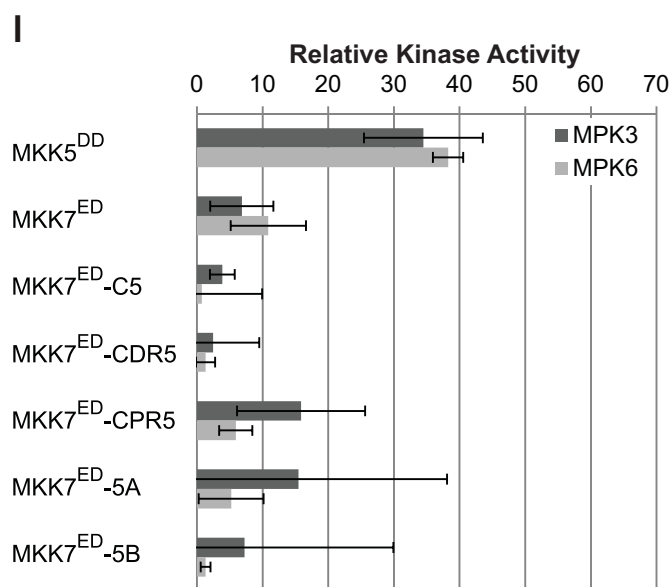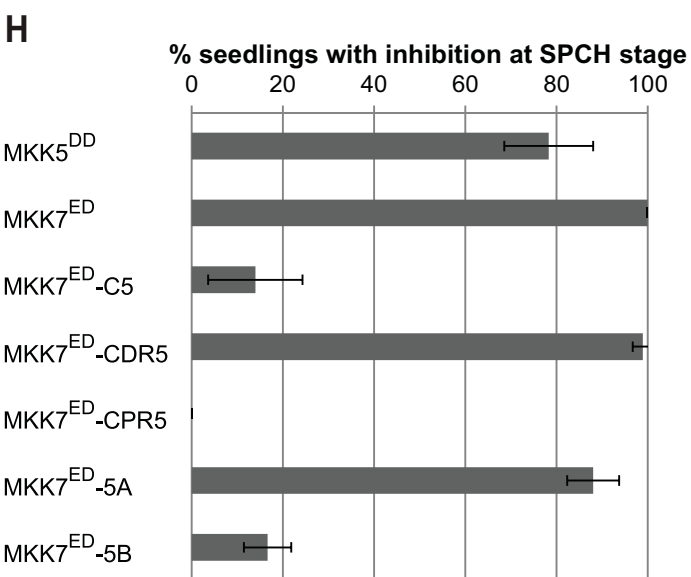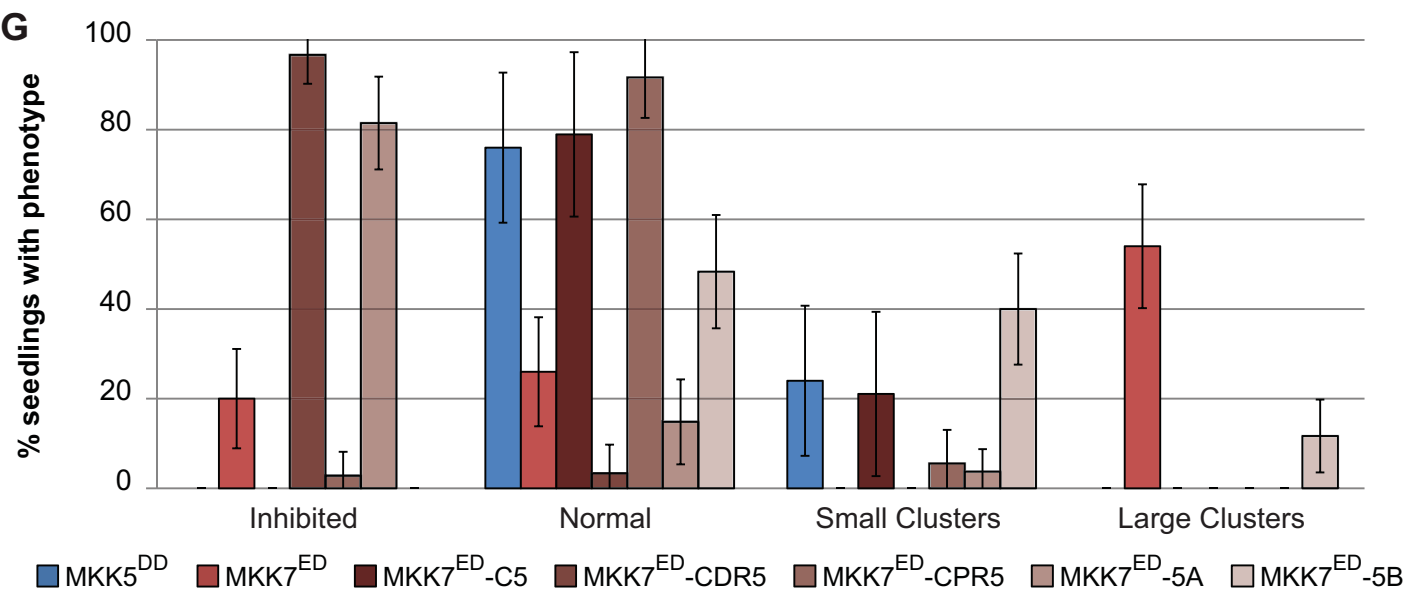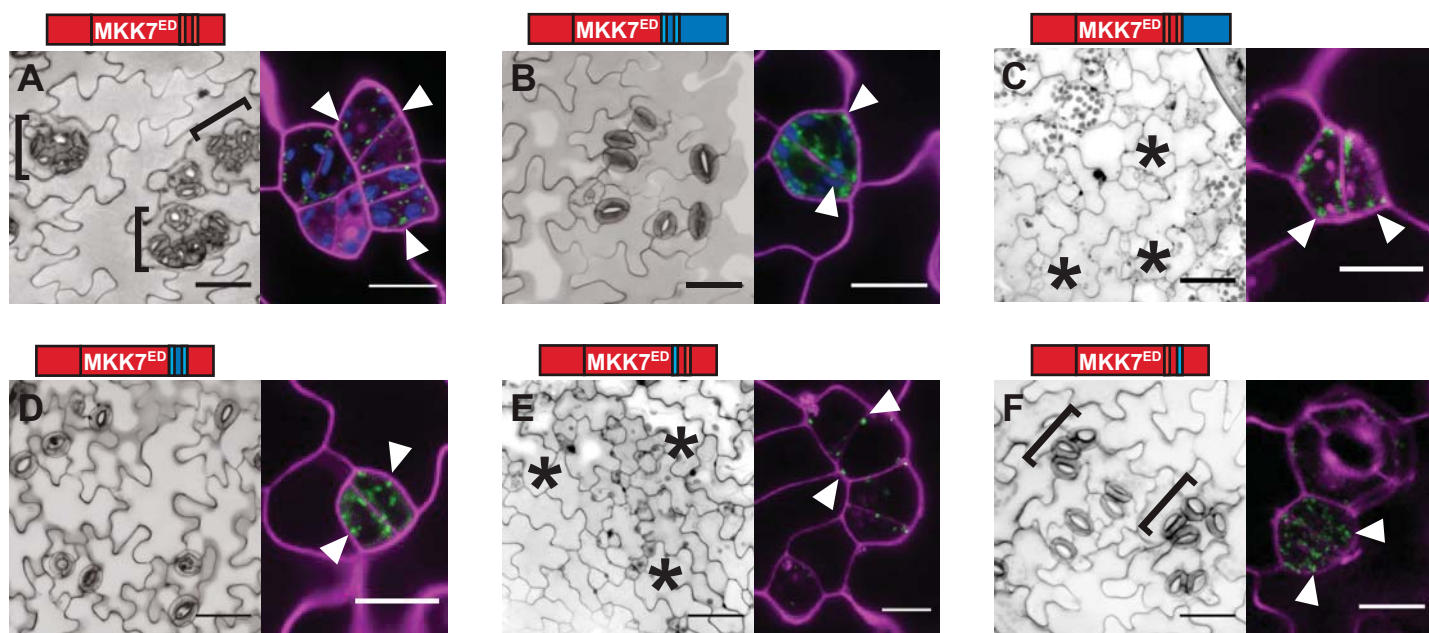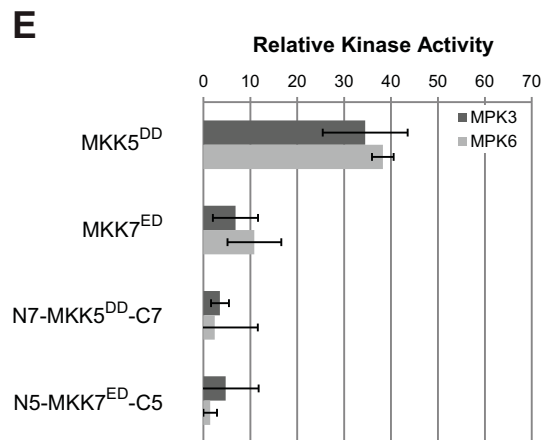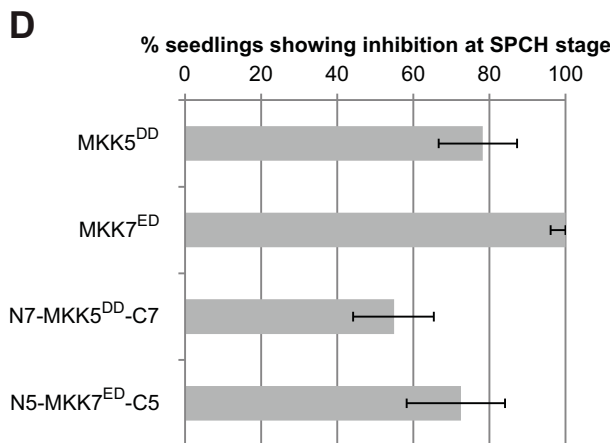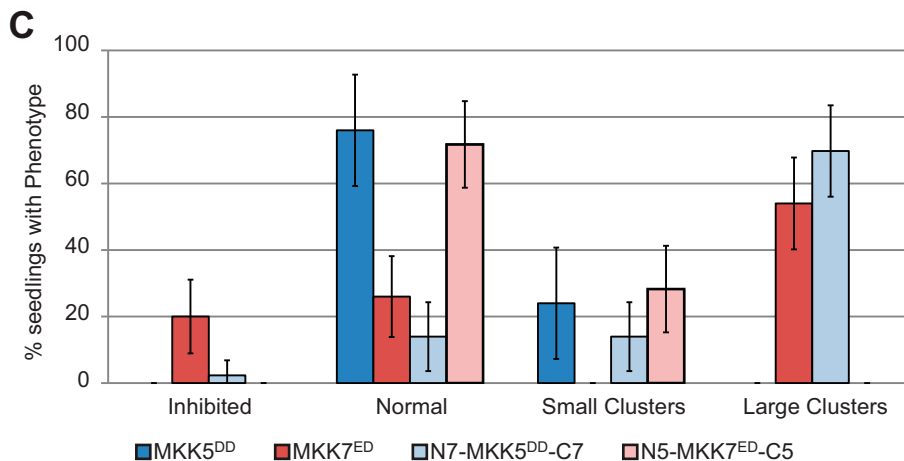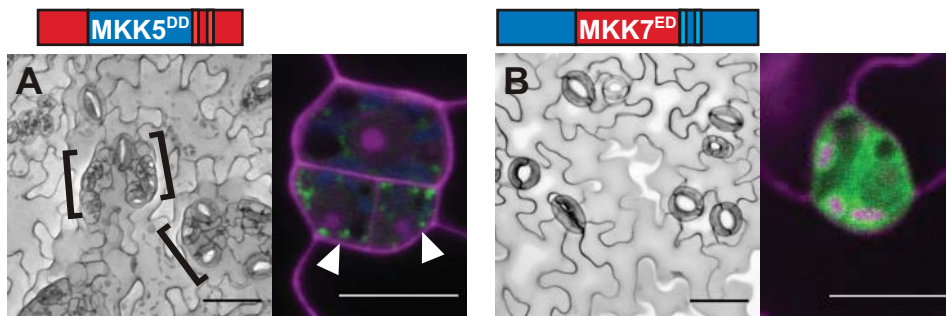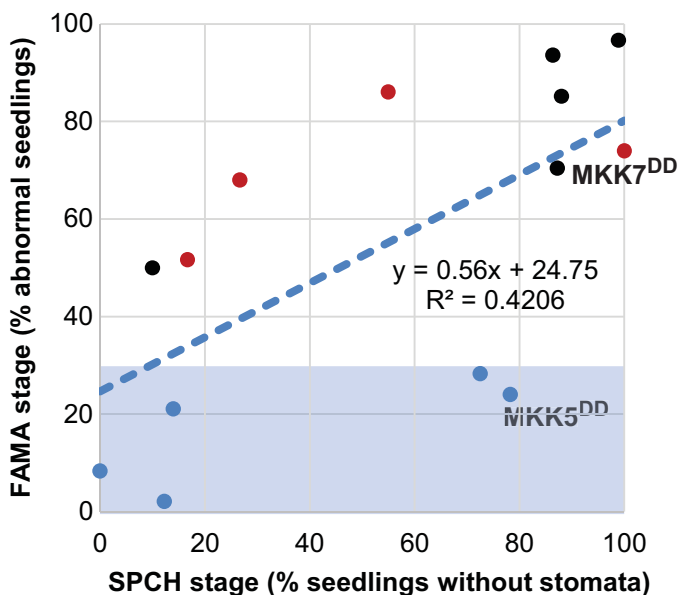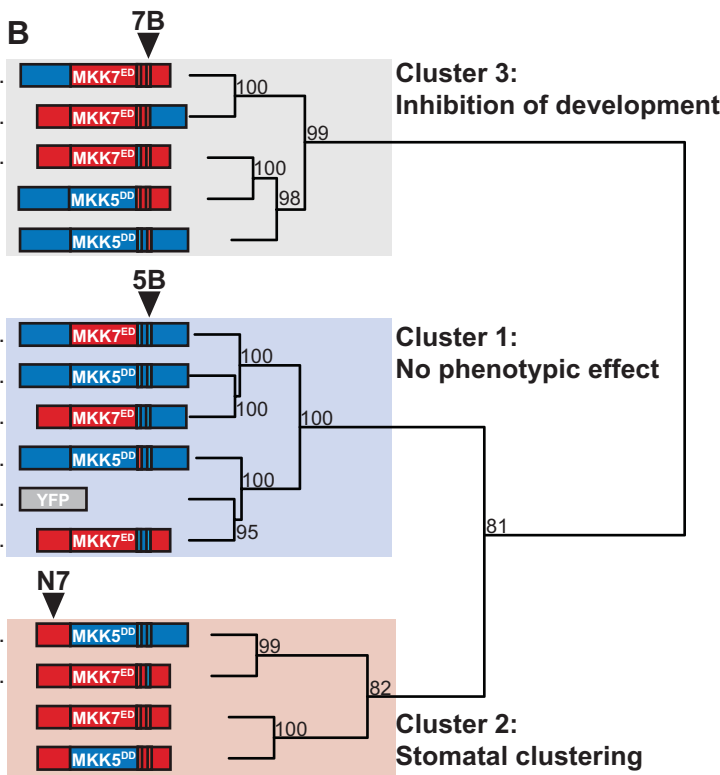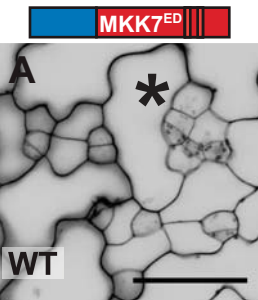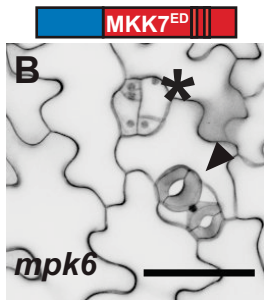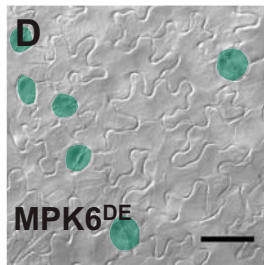
Figure 8

Figure 9

A

Pathways activated by MKK7

B

Endogenous Pathway

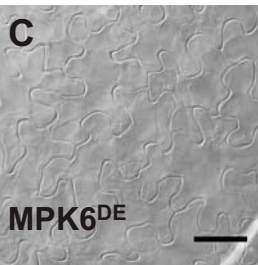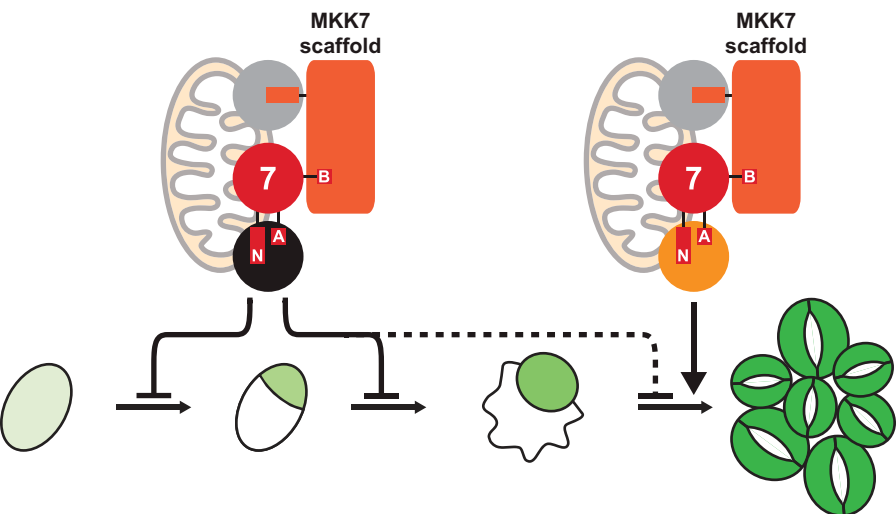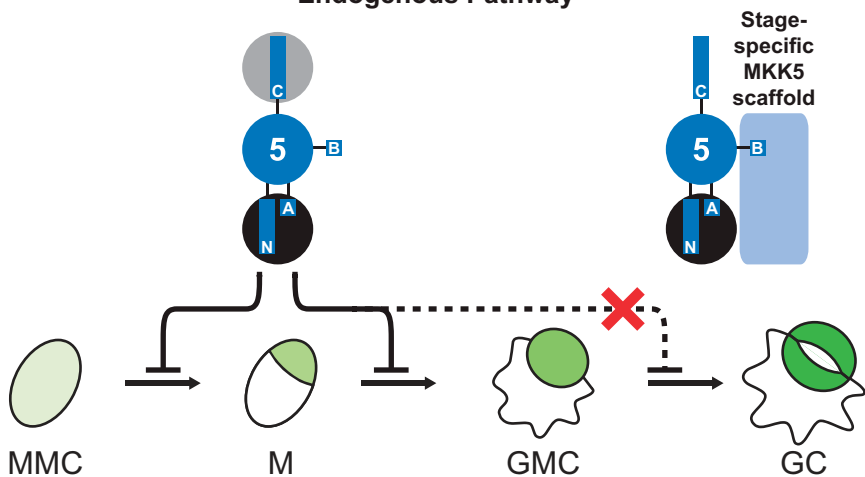MMC   M   GMC   GC

DEVELOPMENTAL SIGNALS

DEFENSE AND STRESS RESPONSES